DYNAMIC ANALYSIS OF BOTTOM HOLE ASSEMBLY
WITH EXTERNAL VIBRATING FORCE EXCITATION

LEI WANG

Dynamic Analysis of Bottom Hole Assembly with External Vibrating Force Excitation

by

©Lei Wang

A thesis submitted to the School of Graduate Studies in partial fulfillment of the requirements for the degree of

Master of Engineering

Department of Engineering and Applied Science

Memorial University of Newfoundland

October 2013

St. John's

Newfoundland

AUTHOR'S DECLARATION

I hereby declare that I am the sole author of this thesis. This is a true copy of the thesis, including any required final revisions, as accepted by my examiners. I understand that my thesis may be made electronically available to the public.

Abstract

As a Vibration Assisted Rotary Drilling (VARD) tool, the newly developed Down-hole Oscillating Device (DOD) is designed for the purpose of improving drilling efficiency. The performance of the DOD was studied theoretically in this thesis. Computational Fluid Dynamics (CFD) simulation is conducted to thoroughly investigate the axial vibration force generated by the DOD. Parametric analysis is then conducted to study whether different drilling fluids can vary the DOD output. Afterwards. dynamic Bottom Hole Assembly (BHA) models are built to evaluate how this additional vibration force affects drilling. In this thesis, both a single rigid body model and finite element model of the BHA are established. Some other simulations are conducted with the finite element model to investigate how various external vibration forces influence drilling enhancement.

Keywords: Dynamic analysis, CFD simulation, Bit-rock interaction, Finite element model, Vibration Assisted Rotary Drilling

Acknowledgements

The author would like to acknowledge the input and support from many people.

First of all, the author would like to express her gratitude to the faculty, staff, and students of the Department of Engineering and Applied Science for making her study at MUN such a great experience.

Then, the author would like to express her thanks to her supervisor, Dr. Steve Butt, for his great guidance; and her co-supervisor, Dr. James Yang, for his constant advice during the last two years.

Also, the author would like to thank other members of the Advanced Drilling Group who were really helpful during her research. They are Farid Arvani, the project manager; Brock Gillis, the Lead Engineer; and all the Colleagues in Advanced Drilling Group. Without all the assistance, she could not get over the difficult problems that easily.

Finally, the author would like to express her special thanks to her family for supporting her all the way here.

Notes on Units of Dimensions

The drilling industry normally uses imperial units to report the relative parameters while SI unit system is employed in some research. In this thesis, SI units are mainly used and other units will be converted. Table 1 shows the conversion between CGS and SI unit systems for some quantities related in this reasearch.

Table 1: Conversion between CGS and SI units in Mechanics

Quantity	Symbol	CGS unit	Equivalent in SI units
Length/Position	L/x	cm	$10^{-2}m$
Mass	m	g	$10^{-3}Kg$
Time	t	s	$1s$
Force	F	$dyne$	$10^{-5}N$
Pressure	P	Bar	$10^{-1}Pa$
Dynamic Viscosity	μ	$Poise$	$10^{-1}Pa \cdot s$

Table of Contents

List of Tables

List of Figures

List of Symbols, Nomenclature or Abbreviations

m = BHA mass

g = Gravity acceleration

M_A, C_A, K_A = Mass, Damping, Stiffness matrices of the BHA element for axial direction

F_A = Axial excitation force

$z, [Z]$ = Axial displacement (matrix) of the system

J_T, K_T, C_T = Equivalent rotary inertia, torsional stiffness, and torsional damping matrices of this dynamic system

T = Torsional excitation torque

$\phi, [\phi]$ = Torsional rotation (matrix) of the system

M, C, K = Equivalent mass, damping, stiffness matrix of the system

F = Equivalent excitation force matrix

k_p = Equivalent spring constant of drill pipe

k_r = Equivalent spring constant of rock

c_r = Equivalent damping of rock

ν_r = Poisson's ratio of rock

ρ_r = Density of rock

ρ_{mud} = Density of drilling mud

r_0 = Radius of rock

$F_{vibration}$ = External vibration force

F_{mean} = Mean value of the external vibration force

F_{amp} = Amplitude of the external vibration force

ω_{vib} = Angular frequency of the external vibration force

F_h = Hook load

N = Hook load proportionality

G = Effective BHA weight

A_p = Vibration Force Acting Area

P_{DOD} = Pressure pulsation from the DOD

A_{cross} = Cross sectional area of drill pipes

D_{co} = Drill collar outer diameter

D_{ci} = Drill collar inner diameter

W_c = Drill collar unit weight

E_s = Young's modulus of drill pipes

E_c = Young's modulus of drill collars

L_p = Length of drill pipes

L = Total Length of the BHA

J = Moment of inertia of each BHA element

l = Element length in the finite element model

G_r = Shear Modulus of the rock

G_c = Shear Modulus of the BHA

s = Surface elevation profile function

s_0 = Initial surface elevation

n_b = Bit factor

$a1, a2, a3, a4, a5$ = Constants in bit-rock interaction model

ω_{bit} = Bit rotating speed

ω_b = BHA Initial Rotating Speed

Z = Regularization function

e = Regularization parameter

μ, λ = Mass, damping proportional Rayleigh damping coefficients

c_c = Critical damping

L_m = Motor inductance

I = Motor armature current

R_m = Motor resistance

K_m = Motor constant

n = gearbox ratio

V_c = Input voltage to the motor

T_{rt} = Torque from the rotary table

ϕ_{rt} = Rotation of the rotary table

f_{BF} = Buoyancy factor

σ_{zz} = Axial stress in the BHA element

$\sigma_{\phi z}$ = Torsional stress in the BHA element for the outer surface

Δz = Axial displacement difference between the two ends of the BHA element

$\Delta \phi$ = Torsional rotation difference between the two ends of the BHA element

$\Delta t, h$ = Time step in central difference method

Δt_{cri} = Critical time step in central difference method

τ_n = Smallest period of a multi-degree-of-freedom system

WOB = Weight on bit

ROP = Rate of Penetration

TOB = Torque on bit

DOD = Down-hole Oscillating Device

BHA = Bottom Hole Assembly

CFD = Computational Fluid Dynamics

PDM = Positive Displacement Motor

DOF = Degree-of-freedom

VARD = Vibration Assisted Rotary Drilling

DPD = Downhole Pulsating Device

BOP = Blowout preventer

Chapter 1

Introduction

Nowadays, more and more advanced technologies are applied to petroleum industry to improve drilling in different aspects: extending bit life, improving drilling efficiency and accuracy, and reducing the cost simultaneously. Normally, vibration in any drilling application is reckoned as a drawback which will bring negative effects to the drilling operation and damage the drill string components[1, 2, 3, 4]. Lots of studies are focused on eliminating the vibration to avoid its side effects. However, little research have been conducted for the attempts to take advantage of those vibrations. The technology of utilizing vibration to enhance drilling is called the Vibration Assisted Rotary Drilling (VARD) technique. Tools designed based on this technology are called VARD tools. The tools are capable of generating axial vibration forces. These forces will then gently oscillate the drill string or the BHA to finally improve Rate of Penetration (ROP) of the drilling. As a result, the vibrations will be benign to drilling process and assist with penetration.

Basically, the VARD tools work with a rotary drill rig system. In this chapter, a brief description of a conventional rotary drill rig system is presented first. The VARD concept is introduced as well. Then, the thesis background, the objective

and significance of this research work, along with the methodology employed in the research will be presented at the end of this chapter.

1.1 Overview of Rotary Drill Rig System

Drill rig system in petroleum industry is normally the massive structure housing equipment used to drill oil-wells, or natural gas extraction wells. Drilling types vary with different applications: for example, auger drilling, percussion rotary air blast drilling, air core drilling, cable tool drilling, reverse circulation drilling, diamond core drilling, hydraulic rotary drilling, and sonic (vibratory) drilling[5]. However, this thesis is focusing on rotary drilling. During rotary drilling, a sharp, rotating drill bit is employed to penetrate geologic formations. Rotary drilling became popular from the success of the well in Texas in 1901. Since then, rotary drilling gains more attention[6].

In any process of drilling, the basic procedures are the same. Whether the well is vertical or directional, oil well or natural gas well, several elementary points are needed for successful and economical drilling. They are: a force acting on a drill bit downwardly, rotation of the drill bit, and circulation of the drilling fluid. The clear explanation is shown in Figure 1.1.

Rotary drill rig for oil and natural gas is comprised of two major constituents: manpower system and hardware system. Manpower refers to those drilling engineers and the operation staff. Basically, the hardware system of a rotary drill rig is made up of the following six main systems: a power generation system, a hoisting system, a drilling fluid circulating system, a rotary system, well blowout control systems, and a drilling data acquisition and monitoring system. Figure 1.2 schematically shows the composition of a rotary drill rig system. Following that the subsystems are introduced.
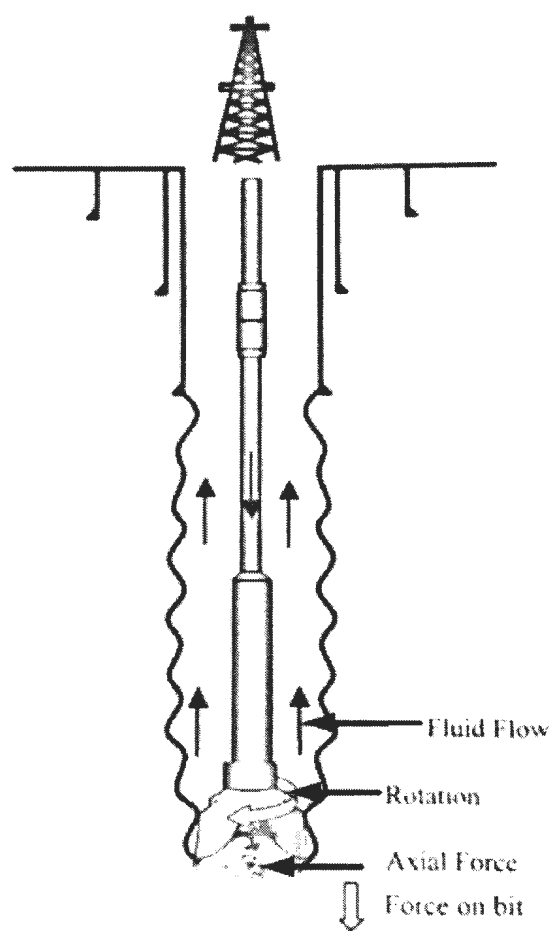
Figure 1.1: Basic Elements of a Drill Rig System[7]
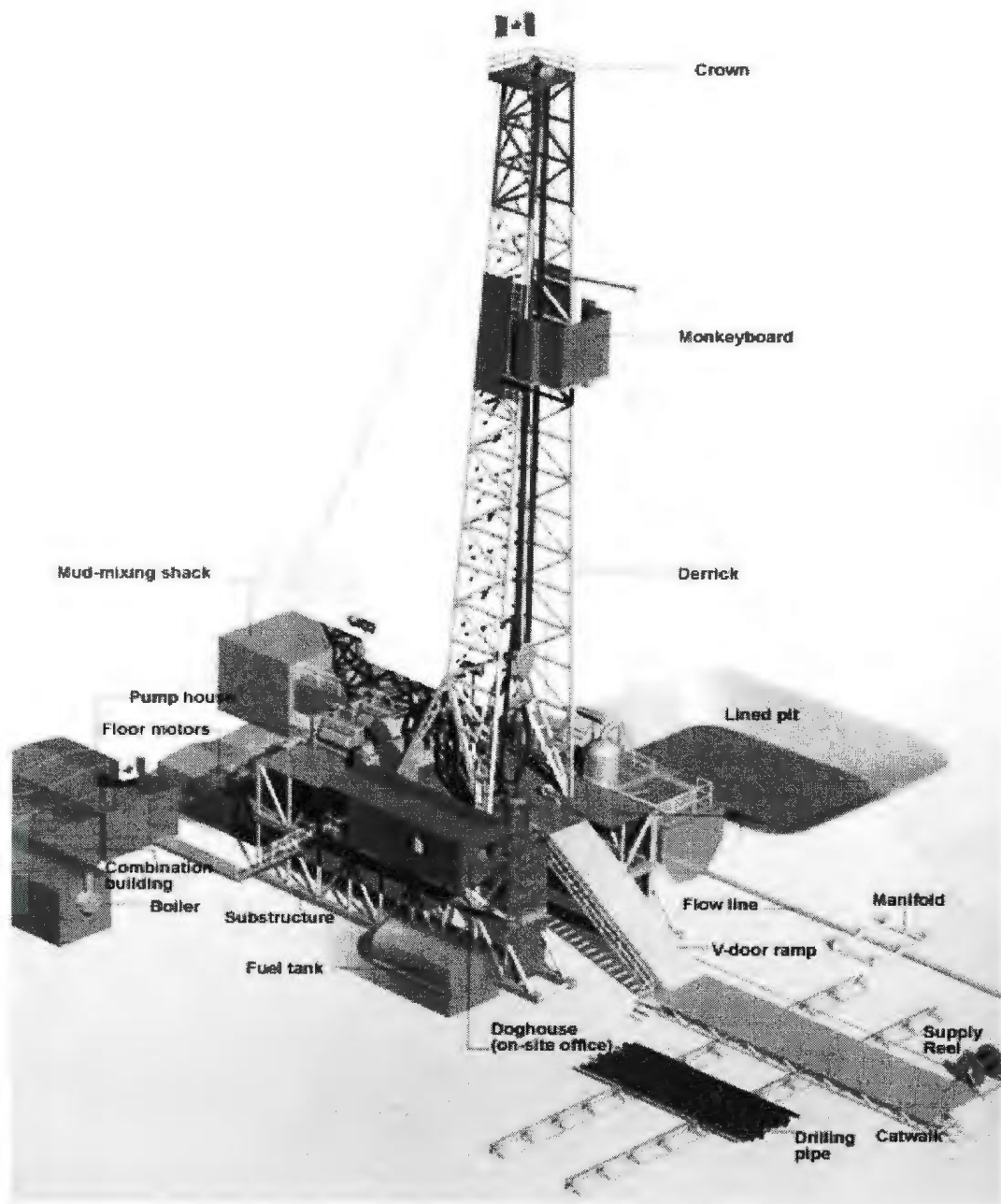
Figure 1.2: Rotary Drilling Rig System[8]

1.1.1 Power Generation System

The power system of a rotary drill rig is designed to supply power for several prime components, especially the rotary system, hoisting system, and drilling fluid circulation system. Furthermore, auxiliaries like the blowout preventer, water pumps, rig lighting system, etc. also have to be powered. The power is generated either at the rig site using internal-combustion diesel engines, or taken as electric power supply from existing power lines[7].

1.1.2 Hoisting System

The hoisting system in rotary drilling is designed to hoist the drill pipes and casing strings during drilling and casing operations[7]. The major components of this system are the draw-works, the crown block, the traveling block, the hook, the drilling line, and the elevator. Figure 1.3 describes how all the parts are assembled a hoisting system.
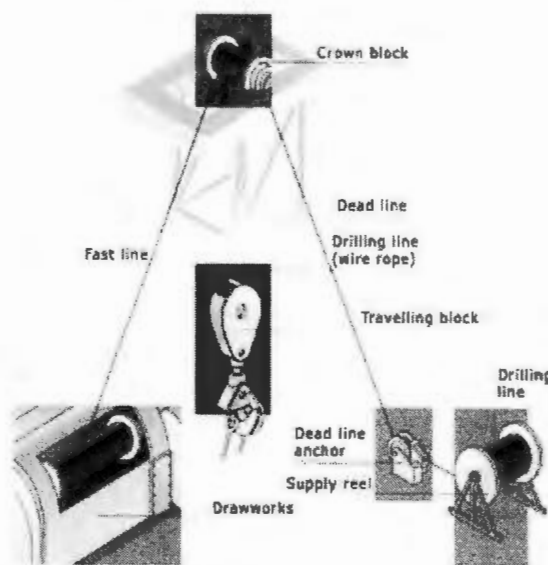
Figure 1.3: Hoisting System[9]

1.1.3 Drilling Fluid Circulating System

Normally, heat and rock cuttings are continuously produced in drilling operations. During any drilling operations, drilling fluid circulates through the drill bit when it cuts through rock. It is proven that drilling fluid is able to lubricate the bit, remove rock cuttings, stabilize the wall around the hole, and control the pressure in the well bore[10]. The drilling fluid is usually a suspension of chemicals and minerals such as bentonite clay in water or sometimes oil. This mixture is blended in the mud-mixing shack. Afterwards, the mixed fluid is pumped up to the standpipe and into the drill pipe through the kelly by a mud pump. The drilling fluid finally reaches the drill bit, cools down the drill bit and flushes rock cuttings. After that, the circulation flows back to the surface through the well bore annulus. When reaching the surface and then going through the shale shaker, the cuttings can be separated from the drilling fluid. The drilling fluid is recirculated after being desilted[10]. As so, the circulation of the drilling fluid is repeated continuously. Figure 1.4 is a picture of the circulating system. The main components are marked out in the figure.

1.1.4 Rotary System

There are two types of rotary systems: the kelly system and the top drive system. Kelly drive system is the older one of the two rotary systems. As shown in Figure 1.5, the components include swivel and swivel bail, the kelly, kelly bushing, rotary table, and master bushing[11]. A kelly drive employs a section of pipe with a polygonal or splined outer surface. This part of pipe then passes through the matching polygonal or splined kelly bushing and rotary table[12]. Since they are matched to each other, when the rotary table on the rig floor rotates, the kelly can be rotated with the drill pipes connected by kelly bushing. This rotation leads to the rotation of the following
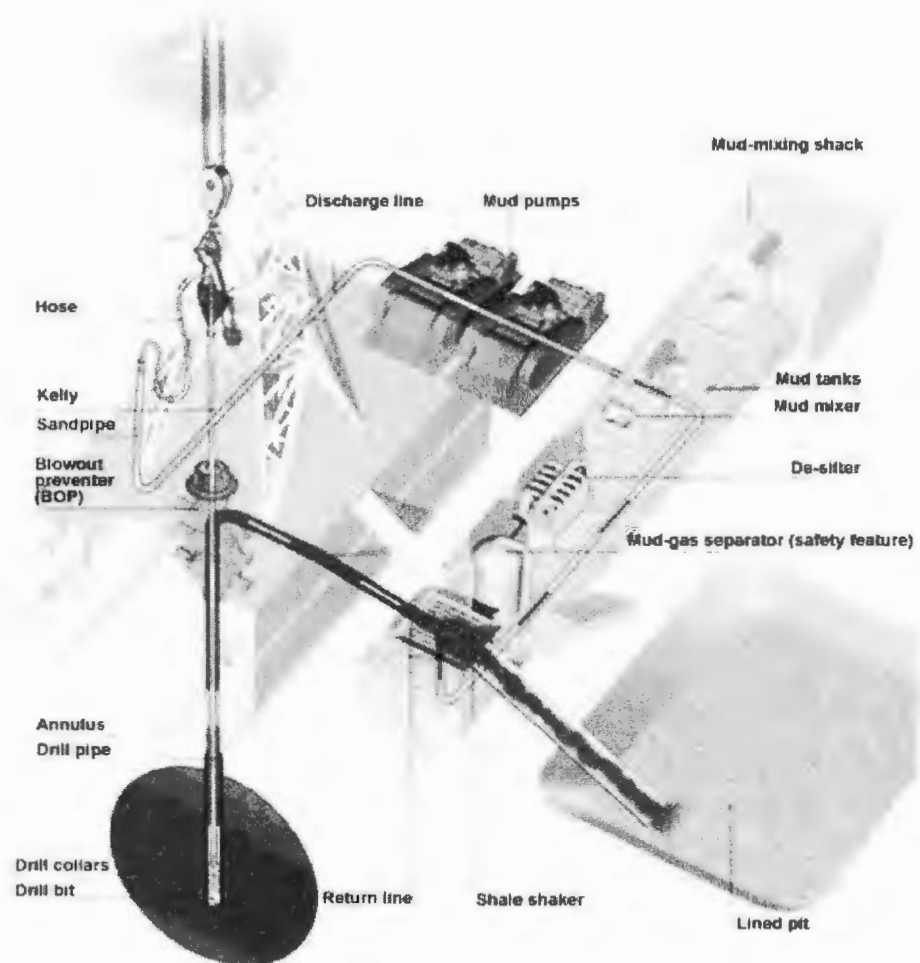
Figure 1.4: Drilling Fluid Circulating System[10]

drill pipes and drill bit.
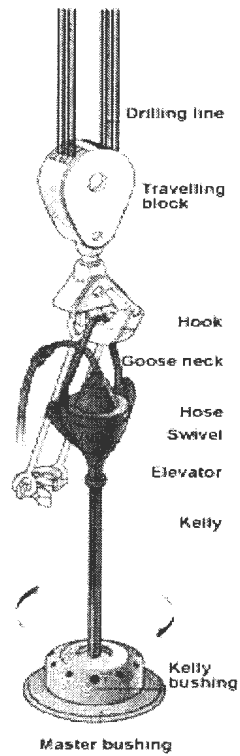
Figure 1.5: Typical Kelly Drive Arrangement[11]

Another rotary system is the top drive system. Figure 1.6 shows the top drive system[11]. In this system, hydraulic or electric motors suspended above the drill pipe are employed to enable top drives to rotate and pump continuously while drilling or during the removal of drill pipe from the hole[11]. Compared to the kelly system, the mechanical equipment of a top drive is located at the swivel and allows a vertical movement up and down along the derrick[13]. With the usage of motors, improvements of the efficiency are observed. Therefore, most offshore units and an increasing number of land rigs use top drives these days.
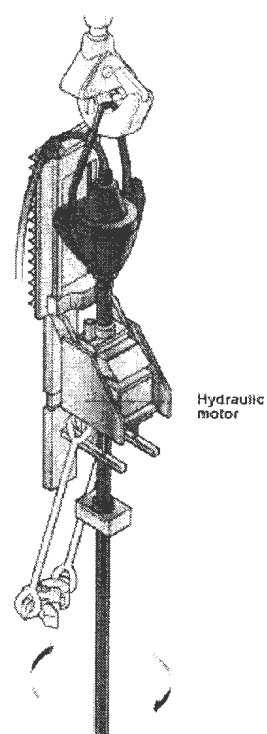
Figure 1.6: Typical Top Drive Arrangement[11]

1.1.5 Well Blowout Control System

A blowout in an oil-well is the uncontrolled release of formation fluids after pressure control systems have failed[14]. Blowouts can induce severe consequences. Therefore, the well control system becomes essential in well drilling applications. The basic components of a blowout preventer (BOP) are illustrated in Figure 1.7. As shown in the figure, the blowout preventer stack comprises of an annular preventer, ram preventers, spools, internal preventers, a casing head, flow and choke lines and fittings, kill lines and connections, mud-and gas-handling facilities, and accumulators[7].
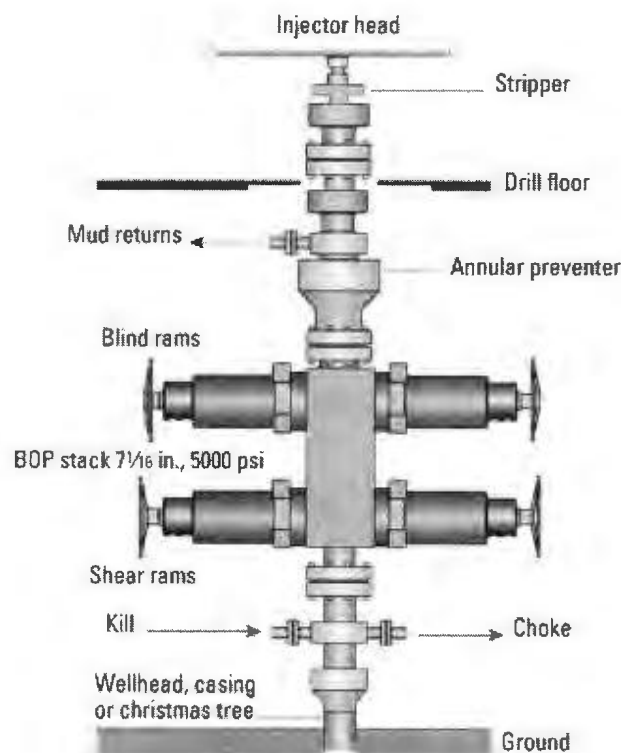
Figure 1.7: Blowout Preventer Stack Components[15]

1.1.6   Drilling Data Acquisition and Monitoring System

During the drilling application, various parameters should be measured or monitored to assure its normal operation. All these parameters are valuable information for drilling. The critical variables includes drilling rate. hook load, hole depth, pump pressure, flow rate. torque, rotary speed. mud density. temperature, salinity, flow properties. mud tank level, pump strokes, weight on bit, hoisting speed, etc. [7] These variables can be monitored, analyzed, displayed, and recorded by certain devices, the so-called data acquisition and monitoring equipment. This system can assist in detecting lots of drilling problems: loss of circulation, well kicks, pipe sticking, drilling breaks. bit bearing failure, high concentration of drilling cuttings, and even blowout.

1.2   Vibration Assisted Rotary Drilling (VARD) Introduction

As mentioned before. VARD technique is the technology of utilizing vibration to enhance drilling. It is important is to create benign axial vibration forces to gently oscillate the drill string or the BHA. The objectives of the improvement in drilling are in many aspects, such as ROP, buckling, sliding, erratic reactive torque, poor tool face control, oriented drilling with steerable motors, high tortuosity and extended reach drilling applications[16]. VARD technique is now considered to be a quite promising technology. As a result, the designs of VARD are rapidly developed. Later in this thesis. the design of VARD tools and their field/lab scale tests and simulations will be introduced.

1.3   Thesis Background

This research work concentrates on the computer simulations of the BHA to predict the additional VARD tool's influence on drilling. As mentioned before, the VARD tool is designed to enhance drilling. A few field/laboratory scale tests have been implemented. However, no detailed theoretical investigation has been conducted on the tool's performance. As so, both single rigid body model and finite element model of the whole BHA system are established. Therefore, this research work will cover the insufficient study on the VARD tool evaluation. Besides, additional simulations are conducted to investigate how various external vibration forces affect drilling.

1.4   Objective and Significance

The main objective of this thesis is to develop appropriate dynamic models of the BHA to evaluate a VARD tool's influence on drilling. The results obtained from the simulations will have to be clearly analyzed and discussed to achieve the evaluation on the tool's performance. The performance should include its influence on rate of penetration, the weight on bit, and even the axial and torsional stress inside the whole BHA. Therefore, simply with a PC, fast predictions and evaluations of the tool performance are available. Compared to field tests, time and cost will be dramatically reduced. Also, from the simulation results, the critical parameters to optimize the tool's design will be known. This is extremely good for the tool's future design. Besides, the successful evaluation of a typical tool sets an example for other similar work. As a result, the evaluation process can be applied to other additional drilling tools.

1.5 Methodology

In this thesis, the typical VARD tool employed in the research is the Down-hole Oscillating Device (DOD). To investigate how it assists in drilling, a series of simulations are conducted in the research.

Based on the working mechanism of the DOD, a 3-dimensional model of its core component, the valve assembly, is built in SolidWorks 2010 software. This model is saved as STL files and then imported into FLOW 3D 2010 software to simulate the assembly's operation. This is Computational Fluid Dynamics (CFD) simulation. The simulation results will predict the pressure pulsations created by the DOD. The data is stored for later simulations with the dynamic BHA system.

The next step is to investigate how the tool affects drilling performance. For this purpose both single rigid body model and finite element model for the BHA are built. The former model only considers the axial translation motion. Therefore, the simulation results can only tell the tool's influence on the rate of penetration and weight on bit. On the other hand, the axial translation and torsional rotation of the BHA are coupled together in the finite element model. As so, the torsional influence can also be known from the simulations with this model. Besides, the stress distributions in both axial and torsional directions are available too. All these simulations are conducted with MATLAB.

To investigate how the characteristics of the external vibration forces affect drilling, some other simulations with the finite element model are conducted. The vibration force in this case is assumed as a simple harmonic force and the parameters of this vibration force are varied in the simulations. Those parameters include the force mean value, amplitude, angular frequency, and even the location where the force is applied.

This chapter briefly introduces the composition of a rotary drill rig system as well

as the development and application of VARD tools. Afterwards, the research work background, its research object and significance, and also the methodology for the investigation are all provided. In the next chapter, the literature review on different VARD tool mechanisms, Computational Fluid Dynamics application in drilling, and the dynamic analysis of the BHA is described in detail.

Chapter 2

Literature Review

2.1 VARD Tool Working Mechanisms Review

There are several mechanisms which can be applied to VARD tools. These mechanisms include hydraulic cavitation. changeable communication area in flow line, and even mechanical vibration mechanisms like percussive hammer. Tools may be designed on those different mechanisms. However, the purpose is quite similar: generation of appropriate oscillations along the drill string. The oscillations are used to gently vibrate the drill string to help improve drilling efficiency by improving ROP. In the following section, different working mechanisms which can be employed in VARD tools are discussed.

2.1.1 Hydraulic Cavitation

Cavitation is the formation and then immediate implosion of cavities in a liquid. Also, cavitation is the consequence of forces acting upon the liquid. This kind of phenomenon usually occurs when a liquid is subjected to rapid changes of pressure which may cause the formation of cavities where the pressure is relatively low. Inertial

cavitation is the process where a void or bubble in a liquid rapidly collapses, producing a shock wave. It can occur in control valves, pumps, propellers and impellers.

In view of these benefits, hydrodynamic cavitation tools are proposed to be a kind of vibration-rotary drilling method. These tools can create longitude vibration accelerations. Actually, the tools are powered by pressurized well bore fluids which are supplied through the drill string in combination with a generic pumping system. The strong pulses which are generated hydro-dynamically are by means of resonance waves. Therefore, with appropriate adjustment, they can be tuned for optimum performance in varying drilling conditions. An example of a down-hole, liquid driven cavitation tool[17] is illustrated in Figure 2.1. The drilling tool is designed to couple advantages of both pulsed jet and cavitating jet. When drilling fluid flows through, fluid is modulated to pulse and cavitate. Because of jet pulsation, cavitating erosion and local negative pressure effect, bottom cuttings cleaning efficiency is enhanced and ROP is improved.

1——Body; 2——Elastic collar; 3——Diverting device; 4——Impeller;
5——Impeller shaft; 6——Impeller and shaft sleeve; 7——Cavity resonator
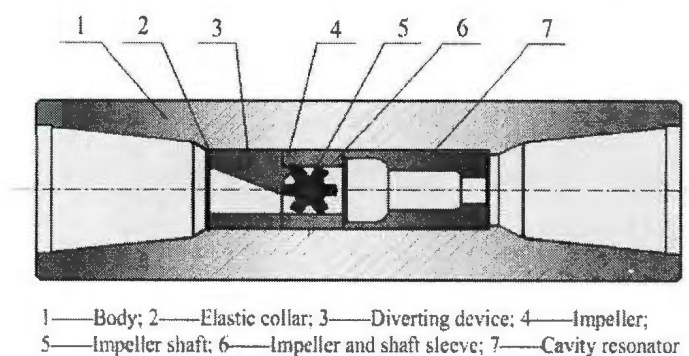
Figure 2.1: Structure of Hydraulic Pulsed Cavitating Jet Generator[17]

As shown in Figure 2.1, this hydraulic pulsed cavitating jet generator is made up of body, elastic collar, diverting device, impeller bed, impeller shaft, impeller and shaft wearing sleeve, and cavity resonator which is also the resonating chamber.

2.1.2 Changeable Communicating Area —— Flow restrictor

The apparatus based on this mechanism usually includes a housing providing a passage for a flow of drilling fluid toward the bit, a stator and a rotor. The rotor oscillates in the axial direction relatively to a stator. Therefore, the oscillation periodically restricts the flow through the passage and creates pulsations in the flow and finally a cyclical fluid hammer effect occurs to vibrate the housing and the drill bit during use. Figure 2.2 is a perspective view of the pressure pulse modulator[18]. In use, drilling fluid flows into the top of the housing through the annular space between the external wall of the supporting structure and the inner walls of the housing and flows through ports of the stator and the rotor. The fluid flows continue past the rear standoff and on to the drill bit. The shaft drives the rotor to interrupt the fluid jets passing through the ports of the stator to generate a coded acoustic signal that travels upstream.
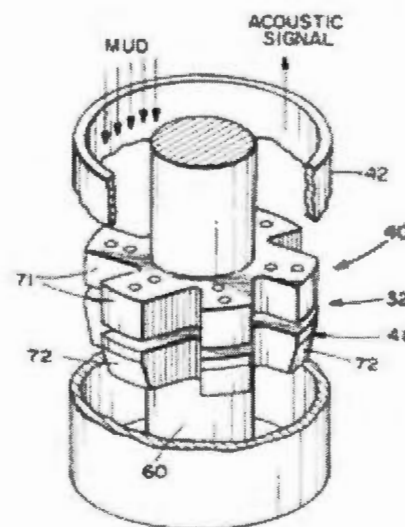
Figure 2.2: Pressure Pulse Modulator[18]

With different configurations of the modulator, different shapes of waves are generated by the apparatus. Figure 2.3 just shows two different configurations of the modulators

with the pulsed shapes generated.
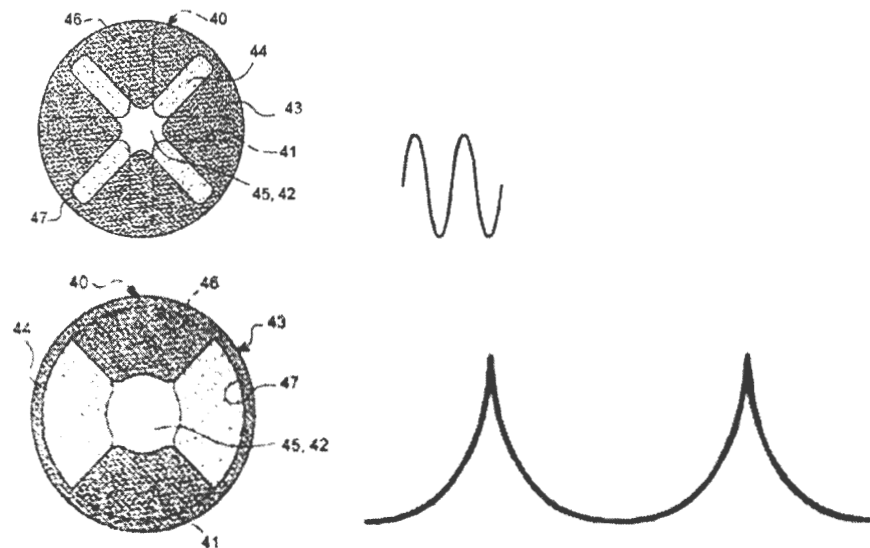
Figure 2.3: Two Different Configurations of the Modulators with their Pulse Shape[18]

Although several embodiments of this kind of modulator have been shown and described above, it is understandable that various changes and modifications can be made. The rotor and/or the stator could have several orifices, the stator and rotor orifices could be different, and of course the shapes shown in the previous figures are not the only possible shapes.

Another example is a Down-hole Pulsating Device (DPD) which was investigated by Nagib *et al.*[19]. When optimizing a drilling system, 4 different parameters would be considered: bit selection, rotary speed, WOB, and hydraulic system. In this case, the authors related one of those parameters to two variations in the operation of the DPD: force generated and transferred to the bit, and the opening ratio of the DPD. The working mechanism here was to partially shut off flow to the tool-face to raise the pressure in the drill string, as a result, exerting more WOB on the bit momentarily. The composition of the DPD is shown in Figure 2.4. The stationary valve assembly

is fixed to the bottom sub, while the oscillating valve assembly was fixed to the rotor of the Positive Displacement Motor (PDM). The connection, zigzag rod, could move the oscillating valve into horizontal displacement with the frequency determined by the rotating speed of RPM. Therefore, pulsating loads were applied on the rotary bit. Nagib *et al.*[19] found a two-parameter, second degree polynomial to be considered as the model of the additional jarring force exerted on the bit which was generated by the hydraulic pulsation action. As a result, it was proven that drilling with a DPD is technically feasible and efficient. It resulted in a higher ROP (72% increase) than conventional drilling technique[19].
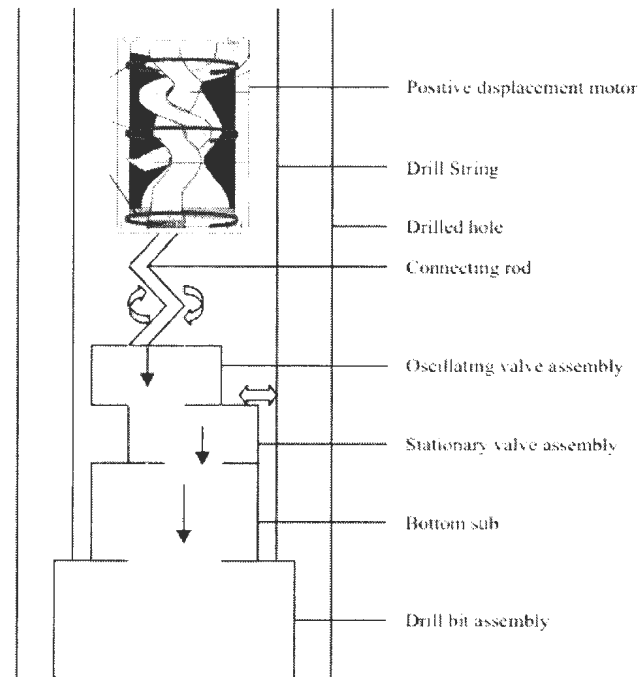
Figure 2.4: Schematic Diagram of a Drill String with a Pulsating Device Attached to the Drill Bit[19]

2.1.3 Mechanical Vibration Mechanism

The down-the-hole vibratory unit[20] for a drilling system includes a casing and a plurality of eccentrically weighted rotor assemblies positioned at least partially with the casing and in fluid communication with the inlet. The eccentrically weighted rotor assemblies can be unbalanced relative to a central axis. Additionally, the assemblies can be configured to rotate in response to a fluid flow directed thereto to apply centrifugal forces to the casing. Figure 2.5 schematically shows how the vibratory unit looks.
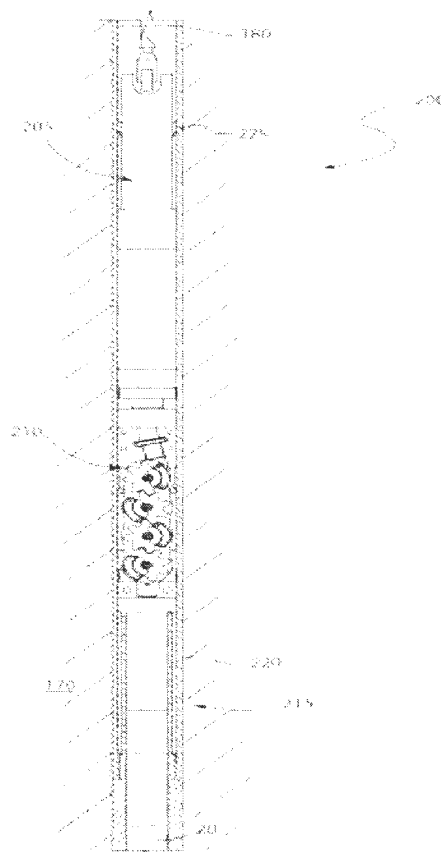
Figure 2.5: A Vibratory Unit and Associated Drilling System[20]

When in the first and third position (from left to right) as shown in Figure 2.6, the

axial components will decrease and the radial components will increase and cancel each other out. When in the second position, there will be the maximum impact force on the bit end while in the last position; there should be the minimum impact force on the bit end. Therefore, the rotation of the rotor assemblies results in cyclical axial forces. Those forces can also be described as vibratory forces. Therefore, cyclical impact force on the drill bit is generated.
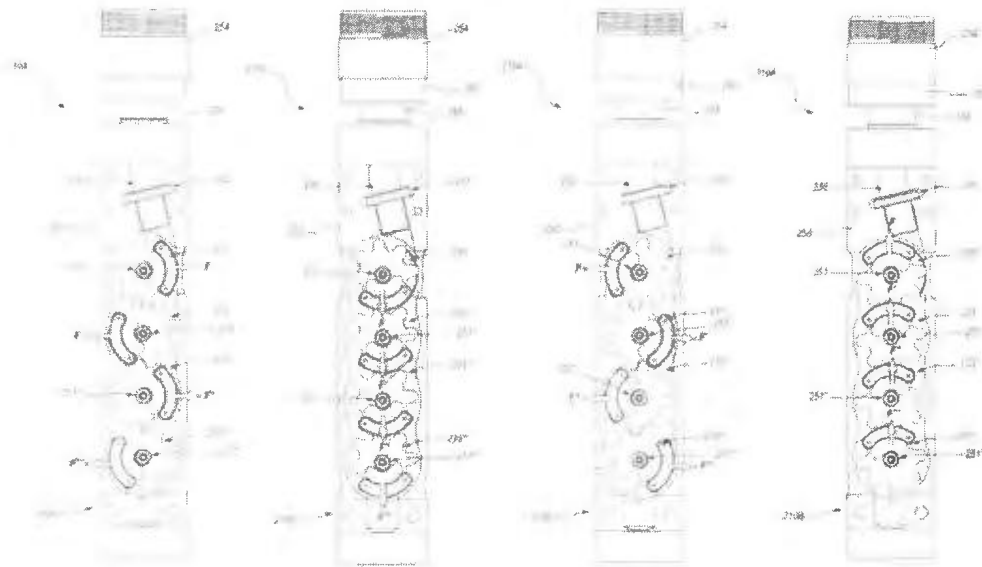
Figure 2.6: A Complete Circulation of the Centrifugal Force Direction Generated[20]

In this research work, the changeable communication area mechanism is employed in the tool of interest. Based on this mechanism, this tool is more simply designed than the tools with other mechanisms. Also, the There are already some available commertial tools based on this specific mechanism. Also, some simple research has been done on this kind of tool. However, there is not enough theoretical investigation into this kind of tool before. Also, having enough knowledge about this tool can help better develop it in the future.

2.2 Computational Fluid Dynamics (CFD) Simulation in Drilling Application

Nowadays, CFD technology has been applied to various situations. Lots of investigations in drilling operations are conducted by CFD. Some of them are introduced in this section.

2.2.1 CFD in Coiled Tubing (CT)

Rosine *et al.*[21] investigated Coiled Tubing with CFD. CT is a practical and cost-effective means when being operated in well intervention in servicing wells. Based on the fact that the actual flow through CT has still not been revealed clearly, Computational Fluid Dynamics is becoming widely used in this investigation[21]. The CFD software employed was FLUENT. Also, SolidWorks was used to build the 3D solid model, and then export the model into GAMBIT software in ACIS format to pre-process. In GAMBIT, geometry is created, meshing is performed, and the boundary conditions are established. As a result, executing a full-scale CFD model can cost significantly less than full-scale testing. Also, the research investigated the fluid flow in both straight and curve sections and the detailed results were then used to evaluate the flow-velocity profile and the flow patterns[21].

Zhou *et al.*[22] also conducted some investigations into CT with CFD software. In their research, there were three different categories of studies: numerical method, fully-developed coiled pipe flow, and boundary layer approximation methods. In the last, they concluded that CFD could be used in both Newtonian and non-Newtonian flow in the curved sections. In addition, comparison between theoretical calculation and numerical simulation are made. The results showed that they agree very well for different flow patterns[22].

The previous successful research on the CT by the CFD software shows the great potential of this research method. And this also set a great emample for part of this research.

2.2.2   CFD of drilling fluid in well bore

Fluid flow in annular spaces has received a lot of attention from oil industries, both in drilling operations and in petroleum artificial lift[23]. The drilling fluid performance in the well bore could be intricate when taking the rotating or non-rotating motion into account. Basically, the inner cylinder rotation would result in two kinds of annuli: concentric annulus and eccentric annulus. Investigations about fluid can be of great complication due to its various properties like density, viscosity, and the state of motion. Better understanding how the drilling fluid performs in the annulus could help know the well condition. Also, using CFD technique, it is possible to make predictions of the pressure profiles and velocities of the drilling fluid. Therefore, optimization of drilling could be conducted more economically, and efficiently compared with experiments.

Neto *et al.*[24] conducted research on the turbulent flows in concentric and eccentric annuli with and without rotating inner cylinder. This research was conducted because of the similarity of the flows occur in drilling operations of oil wells. Five different turbulence models with Reynolds Average Navier–Stokes approach were employed in the simulations. Experimental data from the literature was compared with the predictions[24]. It was found that the simulation results agree well with available experiment data[25, 26].

Pereira *et al.*[23] investigated the flow of non-Newtonian fluids through the annulus. In their research, different aspects for example, viscosity of the drilling fluid, eccentricity of the well bore, flow status, and also the shaft rotation were taken into consideration.

The results obtained in the research were also compared to those in other reported works[23]. At the end of the study, it was proven that the usage of CFD provided satisfactory information or plots about the contours and velocity profiles. Also, the agreement of the numerical method with experimental data from other research work on dimensionless velocity profiles turned out quite good[23].

There were also other comments about the CFD for the drill string section. As mentioned by Saleh *et al.*[27], both mechanical and hydraulic forces acting on the wellbore will influence the drilling operation, for example, drilling efficiency. It was found that the jet force and inertial force have such significant effect that made the hydraulic force became unimportant.

Cui*et al.*[28] developed the governing equations of the helical flow of non-Newtonian fluid in eccentric annuli. Those equations could be solved by using the finite difference method. A secondary flow was formed near the outer cylinder in the largest clearance area. And the region would get larger along with the increase of the eccentricity of the eccentric annulus. The authors also validated the governing equations through the comparison between the computational flow rate of the helical flow and the flow rate measured from an experiment.

All the above research showes that CFD software is a powerful tool to investigate the performance of drilling tools when drilling fluid is involved in. With the software, the fluid performance can be observed clearly. The results can even show the movement of fluid when the research object is in operation. This is the reason why CFD software is employed in this research.

2.3 Dynamic Analysis of BHA/Drill String

2.3.1 Lumped Parameter Model

Yigit and Christoforou[4] investigated the stick-slip and bit-bounce interaction in an oil-well drill string. It is well known that stick-slip and bit-bounce have negative significant effect on drill string and equipment. To study the effects on stick-slip and bit-bounce interactions under various operating conditions, a lumped parameter model with coupled axial and torsional motions was built. Figure 2.7 is a schematic view of the drill rig system studied in this research. It is assumed that the rotary table of the system was driven by an armature controlled DC motor through a gearbox.
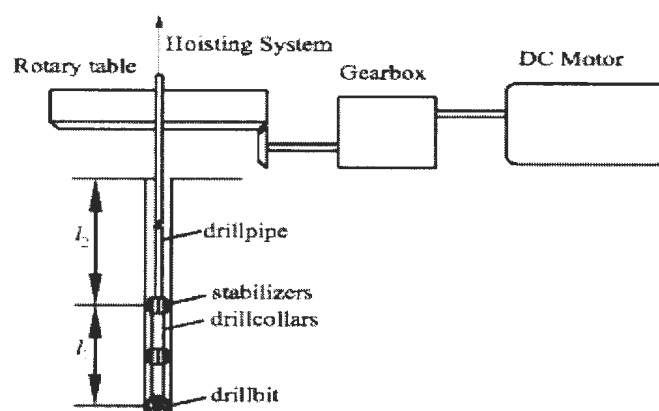
Figure 2.7: Sketch of the Drill Rig System[4]

As mentioed before, this dynamic model contained the mutual dependence of axial and torsional vibrations, as well as the bit-rock interaction. It was proven that bit speed and formation stiffness were the major factors affecting dynamic response. Also, the authors discovered that rotational control alone might not be sufficient to assure smooth drilling under various operating conditions. An additional active controller for the axial motion is needed for effectively suppressing stick-slip vibrations and

bit-bounce once they are initiated.

2.3.2 Finite Element Model

Spanos and Payne[29] studied the dynamic response of a BHA model. In this research, to develop the dynamic model, finite-element technique was employed. The mass matrix was set as frequency-dependent to account for the fluid added-mass effect. Figure 2.8 shows the BHA system and on which the dynamic model was built.
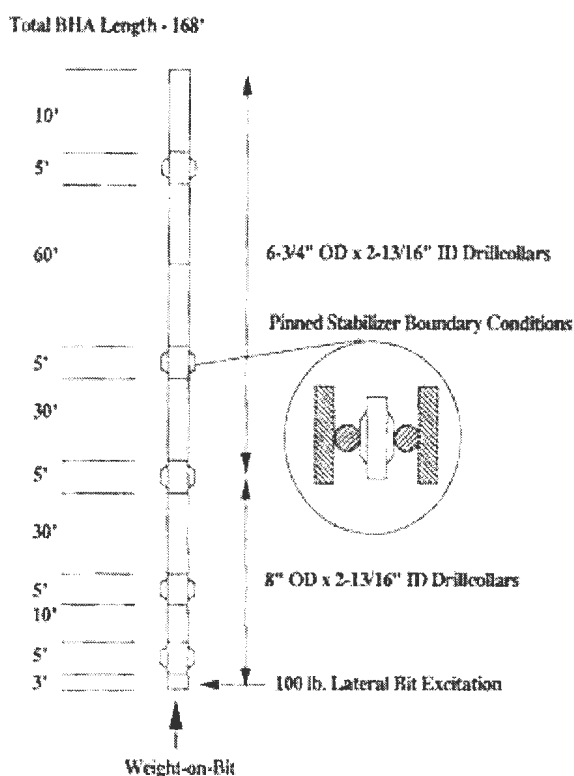
Figure 2.8: BHA System for Numerical Studies[29]

The dynamic BHA model was assumed under monochromatic harmonic excitation. When building the mass matrix of the dynamic BHA system, the added mass effect was considered. Euler-Bernoulli beam theory was used in deriving the stiffness of a

BHA section. The damping was assumed to include Rayleigh damping, structural damping, and viscous damping. The excitation in drilling may come from different sources; for example, there might be bit forces, drill collar mass imbalance, stabilizer loads, and drill pipe kinematics[30]. In this research, only a lateral force applied at the bit with an appropriate magnitude was considered. The lateral stiffness of the drill pipe at the top was assumed to be zero. And the stabilizers were regarded as pinned boundary conditions which would restrict lateral displacement but not rotation. The bit was treated as the excitation node and it is where the lateral force is applied. The authors[29] pointed out that in order to model BHA system more precisely, stiffness of special components and bit excitation spectra should be addressed through laboratory-based testings. And the best result would be achieved from the collection, analysis, and modeling of full-scale field data.

Clayer and Vandiver[31] conducted an investigation on the effect of surface and downhole boundary conditions on the vibration of drill strings. The vibrations were specified as torsional and axial ones. A case study based on a well in southern France was presented[31]. Also, the direct impedance measurements of the drill rig in torsional and axial motion were presented as well. They estimated the boundary condition at the bit in torsional and axial motions. This research work also made comparison between the simulated and measured impedance functions.

The mechanical model of Clayer and Vandiver[31] study is shown in Figure 2.9. The excitation at the drill bit is assumed to be either an axial force or axial displacement applied on the bit.

In this model, the drill string is firstly divided into multiple sections with the same properties. Having the response of each simple section, it is not difficult to get the response of the whole drill string model. The power swivel or top drive was simply modelled with a mass-spring-damper system. The torsional bottom boundary condi-
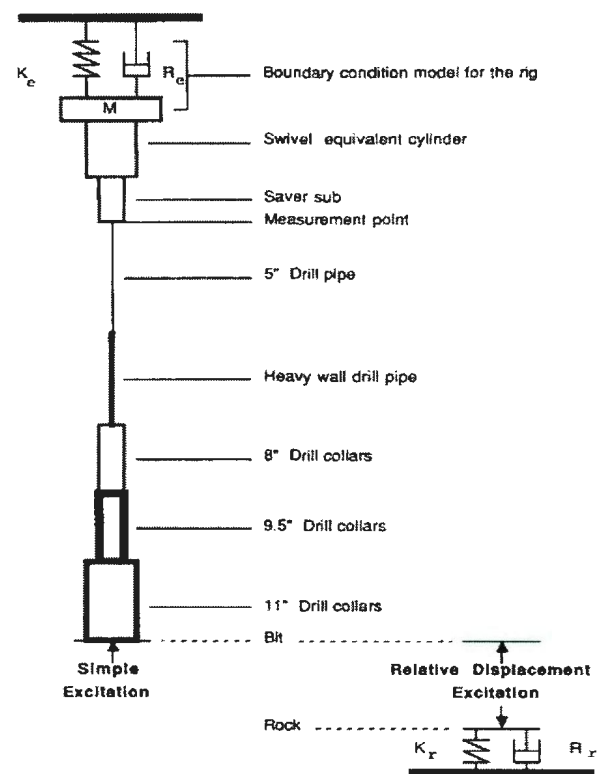
Figure 2.9: Drill String Mechanical Model[31]

tion of this model was a free stiffness end with only damping. As for the axial bottom boundary condition, it is presented by a simple equivalent linear spring and damper model. This model successfully simulated the stiffness and the damping properties of the rock. It was stated that stable BHA resonances might only occur under certain conditions[31].

2.3.3 Bit-rock Interaction Model

Bit-rock interaction is an important topic in the researches about drilling. It is an important composition of a dynamic BHA model. Lots of models have been proposed and a few of them have been applied in dynamic research. In this section, two typical bit-rock interaction models are introduced in detail.

2.3.3.1 Zener Model

Luiz and Franca[32] introduced a bit-rock interaction model for rotary-percussive drilling as well as for conventional rotary drilling. Since the roller-cone bits are characterized by moving roller cones supported by bearings, a relatively high axial compliance is generated. To account for this compliance, the roller-cone bit was modeled as a mass–spring–dashpot system and the rock beneath the bit was modeled as a simple spring. However, this model was not easy to deal with, it is transformed to a more common model called Zener Model or Standard Linear Solid Model. Figure 2.10 shows the original model (left) and the Zener model (right).

Brennan and Carrella[33] presented a consistent and concise analysis of the free and forced vibration of the Standard Linear Solid Model. The authors studied the optimum damping values for the system which was subjected to different types of excitation and also made several comparisons. In the case of free vibration, there were three roots to its characteristic equation. They were two complex conjugates and
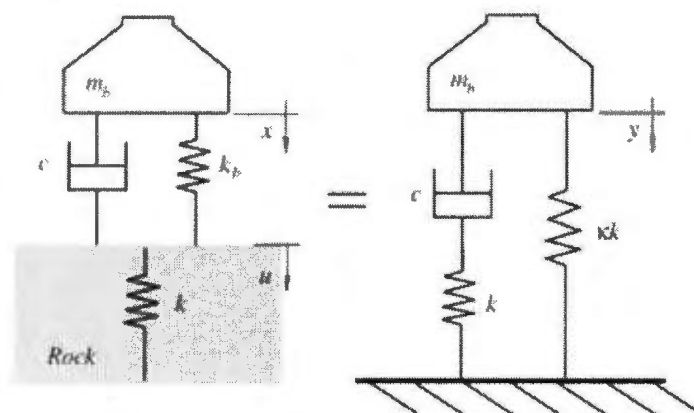
Figure 2.10: Bit-Rock Indentation During Loading (Zener Model)[32]

one purely real root. From their study, achieving critical damping of the complex roots was quite impossible except the case when the additional stiffness was at least eight times that of the main spring. For the forced vibration response, two different kinds of excitation were considered, harmonic excitation and white noise excitation. The studies show that the additional spring offers no advantages when the system is excited by white noise.

Batako and Babitsky[34] illustrated a different bit-rock interaction for impact penetration drilling. Figure 2.11 schematically describes this vibro-impact penetration model into a visco-elasto-plastic medium. This model is comprised of a spring, a dry friction element (plug), and a viscous element. In this system, the spring was mounted in series with the plug, and the viscous element was set parallel to the elasto-plastic element. When the overall forces sustained by the system exceeded the threshold of the force, the bit would have a stepwise downward displacement.

The working mechanism of this model is explained as follows. The striker 4 would firstly impart a blow onto the drill bit 2. Afterwards, the spring 9 and the dashpot 11 would deform gradually due to the visco-elastic properties of the medium. Therefore,
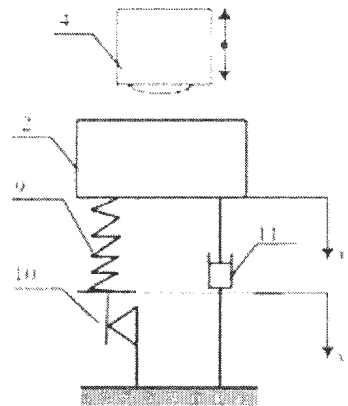
Figure 2.11: Model of Vibro-Impact Penetration into Visco-Elasto-Plastic Material[34]

the bit would oscillate around its initial position of equilibrium defined by the position of the dry friction element 10. However, once overall force became equal or greater than the threshold force, the footing resistance of the medium will instantly change its nature to be plastic without changing the instant position and velocity of the bit. Next, there would be a full compression stage during which the dry friction element slips only in the positive direction of x4 in Figure 2.11. ROP was defined as the drill bit downward displacement in this stage. Also, this full compression stage is ended with a plastic slip when the bit executed a backward restitution stage because of the accumulated elastic energy in the medium[34]. To validate this model, preliminary test drilling was conducted. The results showed that the application of vibration to the drilling process brought an obvious increment in the ROP. Therefore, this result totally supported the concept of percussive-rotary drilling. Furthermore, the test result showed that even at 10–15 Hz the superimposed vibration was able to result in a significant increase in the ROP[34].

2.3.3.2 Foundation Model

Hsieh and Lysmer[35] discovered that when there was external vertical force applied on a massive foundation, its reaction can be represented by a single-degree-of-freedom mass-spring-dashpot oscillator. Later, Lysmer[36] suggested that the stiffness and damping coefficients were both frequency-independent. Their use was acceptable in the low and medium frequency range. This is called 'Lysmer's Analog'. Table 2.1 shows the calibration equations for analysis of circular foundation on elastic half-space[37].This table shows the stiffness and damping calculation method for any kind of foundation.

Richart and Whitman[38] extended Lysmer's Analog and also described that all modes can be studied by employing mass-spring-dashpot systems with frequency-independent parameters which were properly selected. Vertical and torsional oscillations are both axisymmetric. For either of those two oscillations, the cylindrical foundation is investigated with a single degree-of-freedom (SDOF) system. When studying the two anti-symmetric modes of oscillation which are horizontal translation and rocking oscillations, they are coupled with each other. Therefore, the system is characterized as the 2-DOF system. The stiffness and damping values are determined by Table 2.1. As shown in the table, the stiffness and damping ratio are related to the foundation properties. R is the radius of the circular rigid loading area, G, ν, and ρ are all foundation properties and they are shear modulus, Poisson's ratio and density respectively. Besides, I_r, I_z are mass moments of inertia around a horizontal, vertical axis.

The mathematical model Ritto[39] used for the bit-rock interaction was developed by Tucker and Wang [40]. In this model, the axial and torsional motions are coupled together. Also, the calculation equations for ROP and Torque on Bit (TOB) are presented. It is clarified in the model that the ROP depends linearly on WOB and

Table 2.1: Equivalent Parameters for Analysis of Circular Foundations on Elastic Halfspace[37]

Mode	Vertical	Horizontal	Rocking	Torsional
Stiffness	$\frac{4GR}{1-\nu}$	$\frac{8GR}{2-\nu}$	$\frac{8GR^3}{3(1-\nu)}$	$\frac{16GR^2}{3}$
Mass ratio	$\frac{m(1-\nu)}{4\rho R^3}$	$\frac{m(2-\nu)}{8\rho R^3}$	$\frac{3I_x(1-\nu)}{4\rho R^5}$	$\frac{I_z}{\rho R^5}$
Damping ratio	$\frac{0.425}{\bar{m}^{1/2}}$	$\frac{0.29}{\bar{m}^{1/2}}$	$\frac{0.15}{(1+\bar{m})\bar{m}^{1/2}}$	$\frac{0.50}{1+2\bar{m}}$
Fictitious added mass	$\frac{0.27m}{\bar{m}}$	$\frac{0.095m}{\bar{m}}$	$\frac{0.24I_x}{\bar{m}}$	$\frac{0.24I_z}{\bar{m}}$

the bit rotation speed. However, Ritto[39] also put forward the regularization function which is related to the bit rotation speed and a regularization parameter. This regularization is created to avoid the situation when bit speed reaches zero. With this, the TOB would be continuous even when bit speed vanishes[39]. Based on this regularization function, the calculations of TOB and WOB are modified.

However, the bit-rock interaction in real drilling application is very complex. It contains lots of uncertainties. To take those uncertainties into consideration, Ritto[39] developed a stochastic computational model. The general scheme of the drill string system used in this study is shown in Figure 2.12. In this model, a non-parametric probabilistic approach was employed to model the uncertainties in the bit-rock interaction, which is represented by a non-linear operator. The mean model also took the fluid-structure interaction and the impact forces into account. When establishing the model, the authors employed the non-linear Timoshenko beam theory. The non-linear dynamical equations were discretized by means of the finite element method. The probabilistic model presented can successfully work when conducting the simulations

in which a bit loses contact with the bottom-hole rock or the drill string impact on the well-bore. The parametric numerical analysis showed that the non-linear dynamical responses were quite sensitive to uncertainties in the bit-rock interaction model. Furthermore, it was proven that the uncertainties played an important role coupling the axial, torsional, and lateral responses[39].
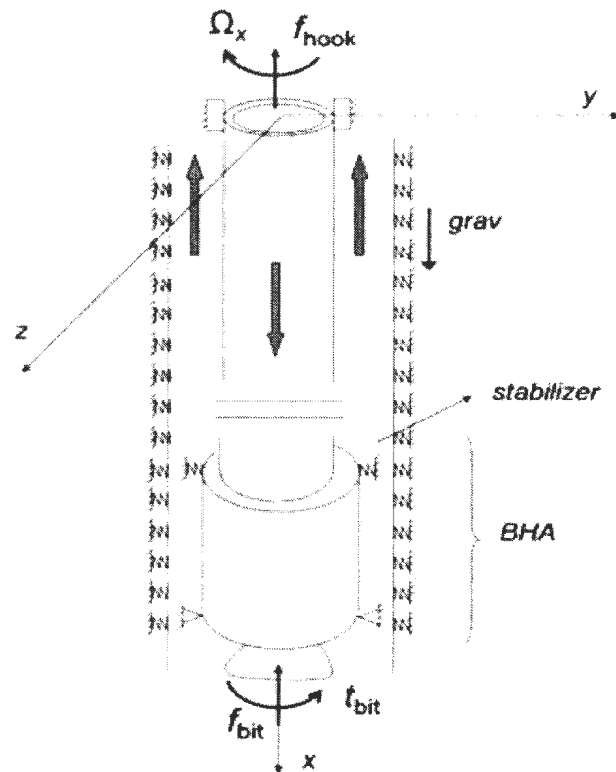
Figure 2.12: General Schemmatic of the Drill-String System[39]

2.4 Field Tests and Lab-scale Experiments on VARD Tools

Franklin and Aref [16] illustrated several case studies of the VARD tool. In the fields of Haynesville, Fayetteville and Barnett Shale Plays, the test results proved that the VARD tool was effective in reducing torque and controlling stick-slip in vertical applications, and directional drilling with down-hole motors. McCarthy[41] pointed out that adding the VARD tool to a drilling system could improve drilling efficiency and keep the compatibility with other drill string components simultaneously. With inclusion of the VARD tool, the vibration of the drill string was increased. For example, in both examples cited above, the maximum of axial acceleration was increased from about 3g without the VARD tool to about 4.5g. This increase in vibration didn't have significant negative effect on the drill string.

Lab-scale experiments were also conducted to study the VARD tool's influence on drilling when adding axial vibration forces to the system. Li *et al.*[42] carried out vibration drilling tests. Figure 2.13 shows the experiment setup for the tests. It is based on a Milwaukee 4079 electrical powered coring drill rig modified to provide constant WOB. Constant WOB is provided by a wheel with hanged weight at side. In the tests, a 2-inch diamond coring bit is employed. The VARD force is generated from an electromechanical axial shaker which is mounted at the bottom of the drill stand. The sensors on the setup indicated that the shaker works at a constant vibration frequency of 60Hz. The shaker's vibration amplitude is controlled by a knob. Figure 2.14 shows the various vibration profiles generated by the shaker. Afterwards, a series of experiments were conducted with medium strength cemented sand samples. The experiments were conducted to investigate how the ROP related to WOB and rotary speed.

Figure 2.13: VARD Laboratory Scale Experiment Setup[42]
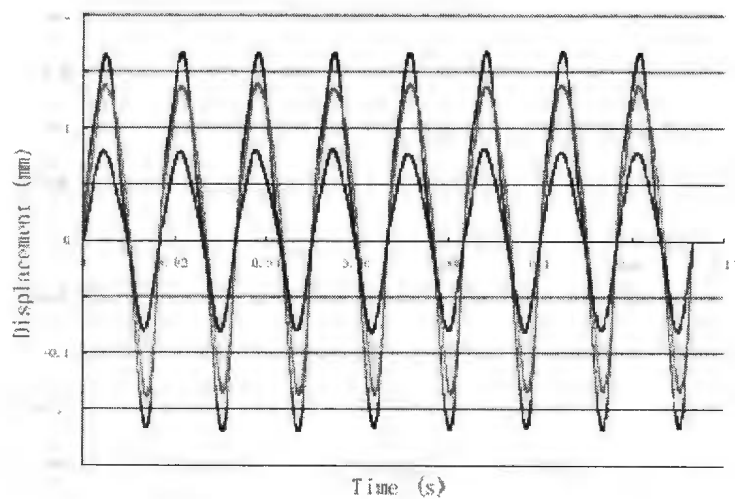
Figure 2.14: Voltage Signals Collected from LVDT Showing Variable Vibration Amplitudes at a Fixed Frequency[42]

The results showed that the drilling penetration rate was increased when drilling with external vibrations. The experiments also indicated that the increase in ROP is accompanied with an increase in vibration amplitude which was approximately linear except when the ROP reached its peak.

Babatunde *et al.*[43] did further investigation on how vibration characteristics influence the drill rate. During the experiments, they varied the frequency and amplitude of the vibrations when drilling with a diamond drag bit. The experiment results proved that the vibration rotary drilling at controlled frequencies did have great improvement in ROP compared to non-vibration drilling. Bit wear was also an important part of this study. However, the experiment results showed that the bit wear was not pronounced enough to create a significant reduction on the overall drilling efficiency.

In summary, this chapter presents literature reviews on nine topics related in this thesis work. The first section is about the study of the working mechanisms which are applicable for VARD tools. Then, the studies about drilling with computational fluid dynamics are presented. Following that, the dynamic analysis on the bottom-hole assembly is reviewed. Finally, both field tests and lab-scale experiments on the VARD tool are presented. Among all the possible working mechanisms, the change-able communicating area is employed. This is because commertial tools based on this mechanism is available. But thoughly theoretical research on the tools is not much yet. They worth investigations. The successful CFD simulation examples show how powerful the software is. Conducting CFD simulations on the tool of interest can show the performance of the tool without huge cost. And the dynamic analysis and experiment instances make the investigation into the tool's influence on drilling possible. All this make the research work be feasible.

Chapter 3

Drilling Oscillating Device (DOD) Introduction

In this thesis work, a vibration assisted rotary drilling tool is studied. The study is focused on its working mechanism, output, and the influence it can make on drilling. More specifically, a down-hole oscillating device (DOD) is investigated for its application in VARD tools. The DOD consists of three main subsystems: excitation section, power section, and operation section. The operation section is a pair of valve plates: an oscillating valve plate and a stationary valve plate. Once the oscillating plate is driven in motion, there will be relative motion between the two valve plates. The power section is usually a positive displacement motor (PDM) which drives the oscillating valve plate into certain pattern of motion. So the operation section is responsible for generating pressure pulsations when the drilling fluid flows through it. The excitation section is designed to transform those pressure pulsations into axial vibration. Figure 3.1 shows the configuration of a typical DOD investigated in this thesis along with an enlarged view of the cross-sectional view of the PDM.

During operation, drilling fluid flows through inside the drill pipes and the BHA. Since
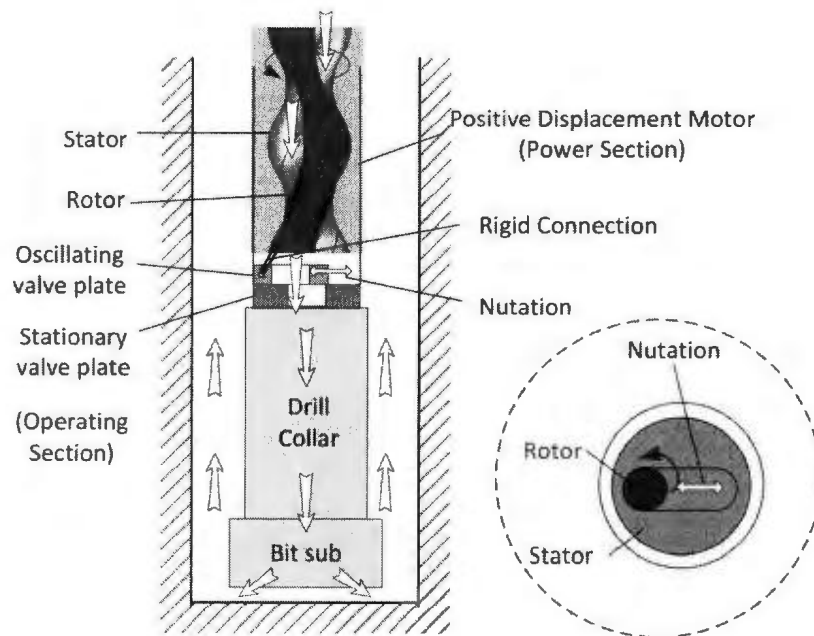
Figure 3.1: Downhole Oscillating Device (DOD) Configuration

the drilling fluid is kept pumping in, the rotor of the PDM will be driven into rotation to transfer the fluid downward. Later, the same rotor can drive the oscillating valve plate into certain movement. As such, there is a relative motion between the two valve plates. This relative motion generates a cyclic change of the cross-section area where the fluid flows through. It means that the flow line is restricted periodically and then pressure pulsations are created. The pressure pulses acts further on the annular load area in the excitation section. Thus, an axial vibration force is generated. The frequency of this axial vibration is determined by the specific configuration of DOD.

This chapter introduces the VARD tool studied in this thesis work: the down-hole oscillating device (DOD). The introduction includes the development and the basic working mechanism of the DOD.

Chapter 4

Computational Fluid Dynamics (CFD) Simulation

To clearly understand aforementioned newly developed tool and how it performs in use, the best way is to directly test it with experiments. However, sometimes conducting experiments is money and time consuming. Therefore, using software to conduct the simulations will assist to evaluate the problem and plan subsequent experiments. As mentioned before, the DOD is basically driven by the pressurized and flowing drilling fluid. As so, the study on this tool is fluid related. In this case, Computational Fluid Dynamics software is chosen for the examination of the chosen VARD tool: the DOD. CFD uses numerical methods and algorithms to solve problems involving fluid flows[44]. It is developed from the first principles of mass, momentum, and energy conservation. CFD software is able to simulate 3-D flows and deals with moving boundary conditions caused by changing geometry[21]. Besides, using software can help create some experimental conditions which are not easy to realize in real experiments. In view of this, CFD simulation with certain software is a good choice in this research work.

4.1 Introduction of the Software

The general-purpose software, FLOW 3D, is employed to conduct the CFD simulations. It can solve the equations of motion for fluids to obtain transient, three-dimensional solutions to multi-scale, multi-physics flow problems[45]. Typically, a numerical model starts with a computational mesh. These generated cells subdivide the physical space into small volumes with several nodes associated with each such volume. After defining the flow parameters at discrete locations, setting boundary conditions and developing numerical approximations, fluid motion equations will be solved. The most traditional numerical algorithms are the finite difference and finite volume methods. There is some difference between the two methods. The finite difference method is based on the properties of the Taylor expansion and on the straightforward application of the definition of derivatives. On the other hand, the finite volume method derives directly from the integral form of the conservation laws for fluid motion and, therefore, naturally possesses the conservation properties[45]. FLOW -3D can be operated in several modes corresponding to different limiting cases of the general fluid equations. Simply speaking, FLOW-3D is applicable for both the modes of compressible flows and purely incompressible flow situations.

To apply the real motion of the valve section, General Moving Objects (GMO) Model is activated in Flow 3D software. GMO is a rigid body under any type of specified physical motion. The motion may be either dynamically coupled with fluid flow or user-prescribed. Normally, it can move with six DOF or rotate about a fixed point or a fixed axis. The GMO model allows users to have multiple moving objects in one problem, and each moving object can have any independently defined type of motion. At each time step, the hydraulic force and torque due to pressure and shear stress are calculated, and equations of motion are solved for the moving objects under coupled motion with consideration of hydraulic, gravitational and control forces and

torques[15].

4.2 Simulation Setup and Results

The 3-D model of this operating section was first built in SolidWorks software. It simply comprised of two valve plates: the oscillating valve plate and the stationary valve plate. In operation, the former plate moves relative to the latter. The detailed configuration and dimensions of the model are shown in Appendix. The 3-D model is saved as STL files and then imported into the FLOW 3D software. The CFD simulation can be conducted. A 3-D model after meshing is shown in Figure 4.1 and the top view of this model is shown in Figure 4.2. The oscillating valve plate is sitting on the top of the stationary valve plate. The boundary conditions of this CFD simulation is presented in Table 4.1. Flow rate in the simulation was set as 946.4 L/min for the inlet and simply outflow at the outlet. The DOD pulsating frequency is 18 Hz. This frequency is related to the configuration of the DOD employed. The speed pattern of the oscillating valve plate is set as ladder-shaped as shown in Figure 4.3. With this speed pattern and the valve assembly profile, the opening ratio of the area where fluid can pass through the valve assembly ranges from 20% (partly open) to 100% (fully open).

Table 4.1: Boundary Conditions in CFD Simulations

Boundary Conditions	
Inlet	Flowrate = 946.4 L/min
Outlet	Outflow
Valve Assembly Opening Ratio	20% (partly open) to 100% (fully open)
DOD Pulsating Frequency	18 Hz
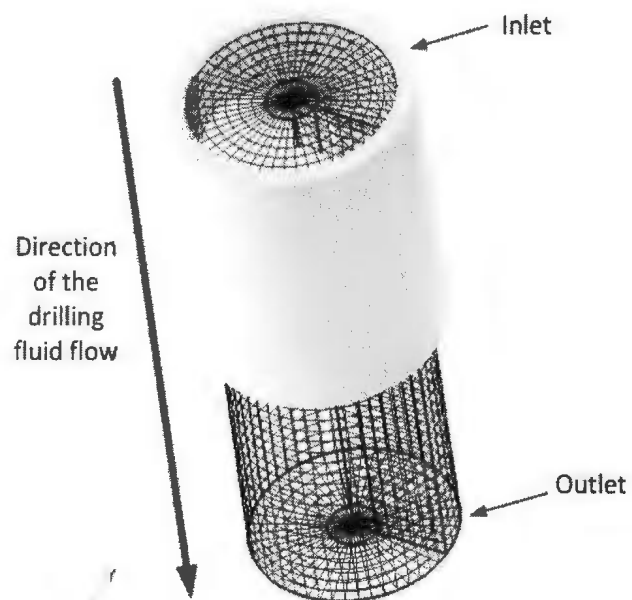
Figure 4.1: Mesh of DOD Valve Part
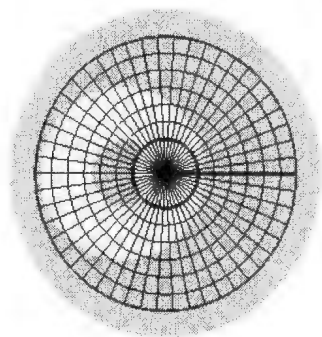
Figure 4.2: Top View of Mesh of DOD Valve Part
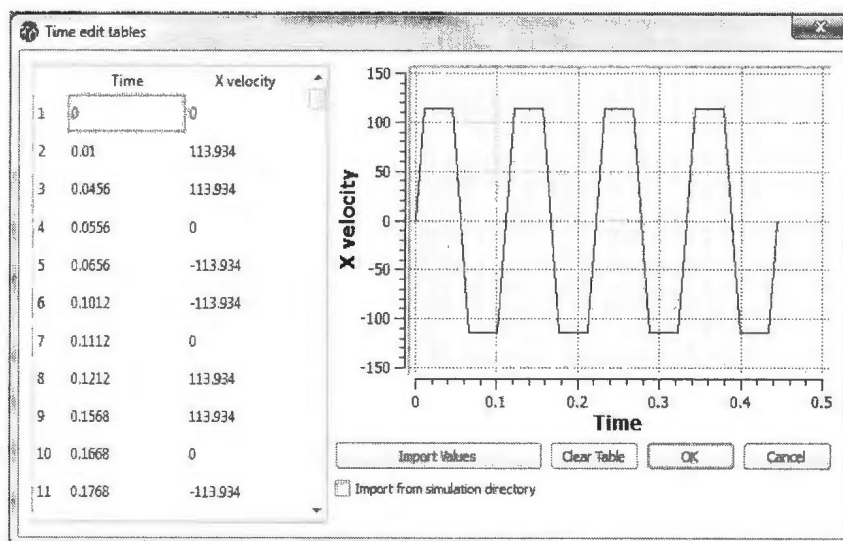
Figure 4.3: Speed Pattern of the Oscillating Valve Plate

Water, as the drilling mud, is firstly used in the simulations. Pressure pulsations are obtained as expected and the plot of pressure versus time is presented in Figure 4.4. The pressure results are measured at the center line of the DOD right above the oscillating valve plate. When the valve assembly is fully open, the the pressure magnitude is the lowest. In this case, the lowest pressure output is assumed to be zero. As shown, the frequency of the pressure pulsations is around 18 Hertz as expected and the peak-to-peak value of the pressure pulsations is about 2.6 MPa. The highest pressure is created when the valve opening ratio is the minimum: 20%. And the pressure is defined as 0 when the valve assembly is fully open. Also, due to some inevitable calculation errors by the software, the peak values in each cycle are not exactly the same. However, it is already enough to collect the characteristics of this output.
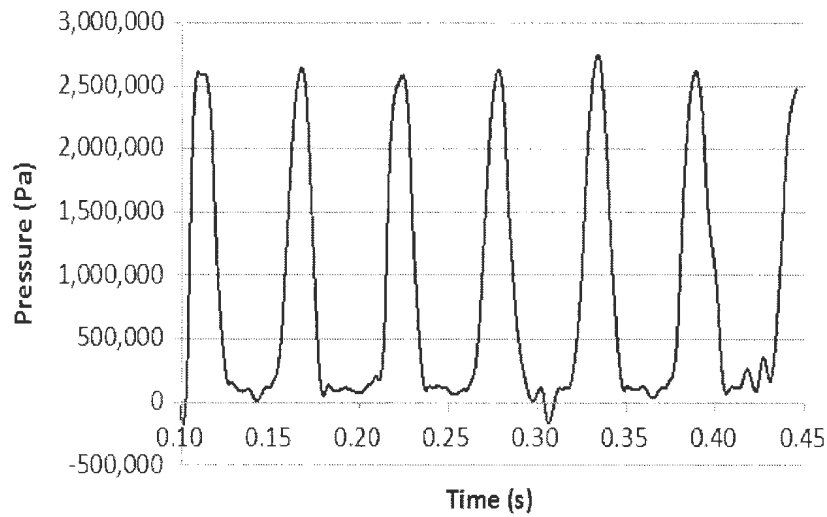
Figure 4.4: Pressure Pulsation from the DOD

4.3 Parametric Analysis on DOD's Performance

It is obvious that drilling fluid properties significantly affect the pressure pulsation. In order to investigate the effect of each parameter, it is necessary to conduct parametric study for the main parameters of the drilling fluid properties. Therefore, drilling fluid with different parameters is simulated. Table 4.2 presents the parameters used in the simulations. As shown, 3 different drilling fluids are used other than water. Different densities and viscosities are studied. The simulation results are given in Figure 4.5. It showed that increasing either density or viscosity of the mud will increase the peak-to-peak value of the pressure pulsation. Besides, density has larger influence compared with viscosity. Water has the smallest density and viscosity; thus, it generates the lowest peak-to-peak value of the pressure pulsation. The detailed simulation results are available in Appendix B.

This chapter introduces the CFD simulations conducted for the valve assembly of the DOD. The software employed is firstly introduced in detail. Afterwards, the

Table 4.2: Variation of Drill Mud Properties in CFD Simulations

Drill Mud	Density (Kg/m^3)	Viscosity $(Poise)$
Drill Mud1	1100	0.5
Drill Mud2	1100	0.1
Drill Mud3	1500	0.5
Water	1000	0.01
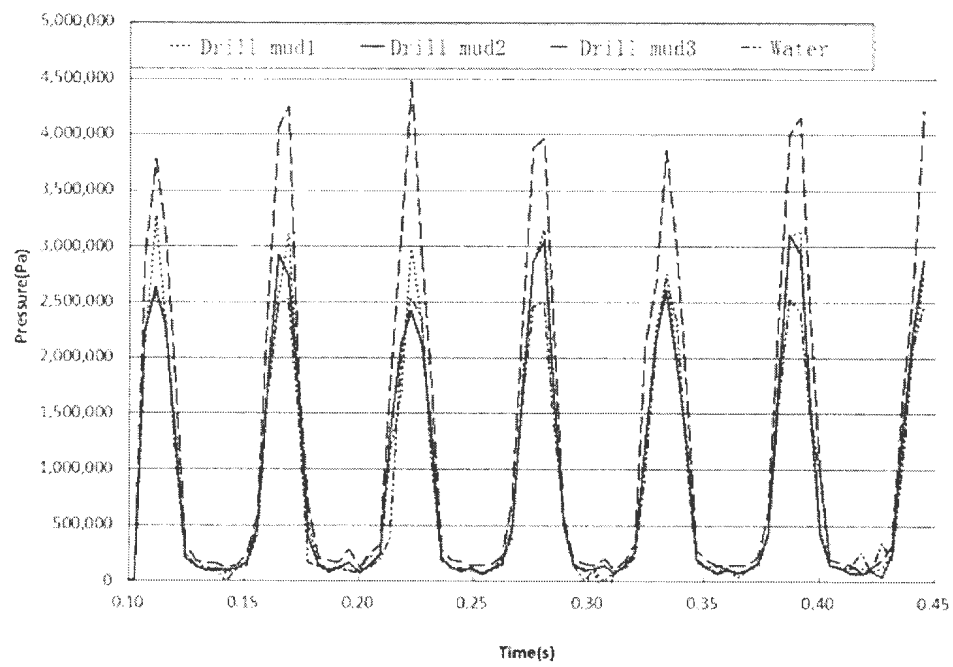
Figure 4.5: Pressure Pulsation Corresponding to Various Drill mud

parameters and boundary conditions setup are explained. A typical simulation is conducted to obtain the output. Also, three other simulations are done with various drilling fluid properties. The results collected in this chapter are set as the input for the dynamic simulations in the next chapter.

Chapter 5

Dynamic Models of BHA and Simulations

In general, the dynamics of the Bottom Hole Assembly (BHA) is very complex and many factors in drilling operation may induce vibrations to the BHA. These factors include bit-rock interaction, drill collar mass imbalance, stabilizer loads, and drill pipe kinematics[29]. In this research work, there is no intention to investigate the BHA dynamics thoroughly. Instead, the interest is mainly in the performance of the external vibration force from the DOD which is installed in the BHA. Therefore, two different dynamic models are built: one is a single rigid body model while the other one is a finite element model. The former is used to roughly investigate how the external vibration force from the DOD affects drilling in just axial direction. The latter is for the further investigations into the stress distribution inside the BHA in both axial and torsional directions. Moreover, it is expected to seek the optimal vibration force which can enhance drilling most with the least side effects. The establishment of the two models and the simulations conducted are introduced in this chapter.

5.1 Simulation with Single Rigid Body Model

5.1.1 Model Introduction

In this section of simulations, a SDOF model with only axial motion is considered. This dynamic BHA model is shown in Figure 5.1. The BHA section is assumed as a 60 meters long rigid steel pipe and the long drill pipe between the BHA and the fixed surface is modeled as a simple spring-damper system. Also, the bit-rock interaction is simulated as a spring-damper system, too. Besides, the BHA is subjected to a constant hook load. The system parameters and excitations are developed later in this section.
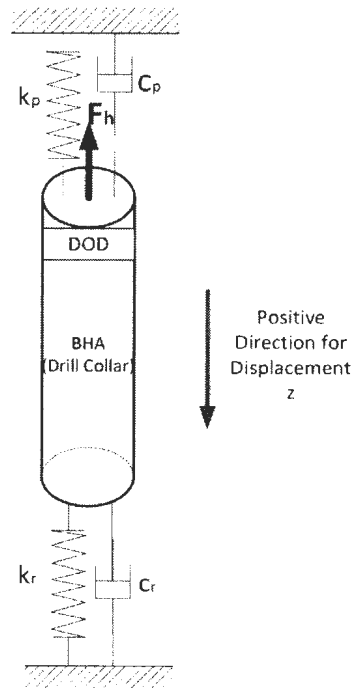
Figure 5.1: General Schematic of the BHA Dynamic System

The governing equation of motion for this BHA model is expressed as below.

$$m\ddot{z} + c_p\dot{z} + k_p z = F_A = G - WOB - F_h \left(+F_{vibration}\right) \tag{5.1}$$

In the equation, m is BHA mass. c_p and k_p are the damping, and stiffness of the long drill pipe respectively. F_A represents the overall excitation in axial direction which includes the effective BHA gravity G, hook load F_h, nonlinear WOB and the external vibration force $F_{vibration}$ generated by the DOD. $F_{vibration}$ is only accounted in the cases where the DOD is installed in the BHA. The definitions of the system parameters and excitation forces are individually introduced as below.

The drill pipe above the BHA is modeled as a spring-dashpot system. The equivalent stiffness k_p of the drill pipe is computed as follows.

$$k_p = \frac{A_{cross}E_s}{L_p} \tag{5.2}$$

where k_p, A_{cross} and E_s are the stiffness, the cross sectional area, and the Young's modulus of the pipe. L_p is the overall length of the drill pipe.

For the equivalent damping of the drill pipe, Rayleigh Damping is employed in this case. It is computed as

$$c_p = \mu m_p + \lambda k_p \tag{5.3}$$

where m_p is the drill pipe mass, and k_p is the drill pipe equivalent stiffness. μ is the mass proportional Rayleigh damping coefficient, and λ is the stiffness proportional Rayleigh damping coefficient. The two parameters will assure the damping c_p less than the critical damping c_c since the system is normally under-damped in real application:

$c_p < c_c$. The critical damping is derived from the following equation.

$$c_c = 2\sqrt{k_p m} \tag{5.4}$$

Equation 5.3 shows that the damping result is sensitive to the tuning of the two parameters μ and λ. However, as long as the system is underdamped, the damping does not influence the stable response of the BHA system since no randomness is considered in this research work.

m and m_p are the BHA mass and drill pipe mass respectively. They are calculated as below. The drill pipe and drill collar specifications[46] are listed in Table 5.1.

$$m = W_c L_c \tag{5.5}$$

$$m_p = W_p L_p \tag{5.6}$$

where W_c and W_p are unit weights of the BHA and drill pipe, L_c and L_p are lengths of the BHA and drill pipe.

5.1.1.1 Bit-rock Interaction

As mentioned before, the bit-rock interaction is modeled as a spring-dashpot system with equivalent stiffness and damping. In seeking for those two parameters, Elastic-half-space-analogs[38] are employed. The calibration equations for equivalent stiffness k_r and equivalent damping c_r are developed and shown as follows.

$$k_r = \frac{4 G_r r_0}{1 - \nu_r} \tag{5.7}$$

$$c_r = \frac{3.4 r_0{}^2}{1 - \nu_r} \sqrt{G_r \rho_r} \tag{5.8}$$

where G_r is the shear modulus of rock, r_0 is the contact foundation radius and ν_r is the poisson ratio of the rock.

WOB is the axial force applied on the bit under dynamic conditions. It is developed based on the research of Yigit[4].

$$WOB = \begin{cases} k_r(z - s) + c_r(\dot{z} - \dot{s}) & \text{if } z \geq s, \\ 0 & \text{if } z < s. \end{cases} \tag{5.9}$$

In the above equation, s is the formation surface elevation[47]. This surface elevation is normally modeled with a sinusoidal function.

$$s = s_0 f(\phi) \tag{5.10}$$

$$f(\varphi) = \sin(n_b \phi) \tag{5.11}$$

where n_b represents bit factor. For a PDC bit, n_b is one while for a tri-cone roller bit, it is three[4, 47]. Obviously, this excitation is nonlinear in nature. s_0 is the amplitude of the surface elevation function. When flat surface is the assumption. s_0 is zero.

The ROP can be estimated by the following equation which was originally developed by Tucker and Wang[40].

$$ROP = -a_1 + a_2 WOB + a_3 \omega_{bit} \tag{5.12}$$

where ω_{bit} is the angular frequency of the system. a_1, a_2, and a_3 are positive constants in this bit-rock interaction model. This equation shows that the ROP depends linearly on WOB and the bit rotation speed.

As mentioned before, the nonlinear WOB model indicates that there should be two different natural frequencies of this system. One is for the case that drill bit does not

have contact with bottom hole, the other case is that drill bit has contact with the well bore bottom. The natural frequencies in the two cases are calculated individually as followed. ω_{n1} is the non-contact case, and ω_{n2} is the contact case.

$$\omega_{n1} = \sqrt{\frac{k_p}{m}} \tag{5.13}$$

$$\omega_{n2} = \sqrt{\frac{k_p + K_r}{m}} \tag{5.14}$$

5.1.1.2 Overall Axial Excitation Force

During drilling, the whole BHA is immersed in drilling mud. Obviously, buoyancy will influence the force exerted on the BHA. In order to account for this effect, effective gravity rather than the gravity in air is employed in the model establishment. Buoyancy Factor f_{BF} is introduced when computing the effective gravity. It is related to fluid density ρ_{mud} (Kg/m^3) only[48]. The calculation process is shown below.

$$G = mg f_{BF} \tag{5.15}$$

$$f_{BF} = 1 - 1.83 \, \rho_{mud} \tag{5.16}$$

Where m is BHA mass and g is the acceleration of gravity.

Hook load in drilling is usually defined as the weight of the drill string and associated components that are suspended from the hook. In any drilling case, the neutral point of the drill string should be in the BHA. Neutral point is the point in the drill string where the axial stress changes from compression to tension[49]. This means that at the neutral point, the axial stress is 0. In this case, only the BHA is studied. To assure this neutral point in BHA, the hook load F_h in this case has already canceled

out the weight of the drill pipe. F_h is calculated as below.

$$F_h = NG \tag{5.17}$$

where N is the proportionality coefficient which ranges from 0 to 1 and G is the effective gravity of the BHA. When drilling with the DOD, $F_{vibration}$ should be included in the excitations. It is computed by the following equation.

$$F_{vibration} = P_{DOD} \, A_p \tag{5.18}$$

where P_{DOD} is the pressure result from the CFD simulation and A_p is the area in the DOD where the pressure pulsations act on. Therefore, the axial excitation force is summarised as below.

$$F_A = G - WOB - F_h \left(+F_{vibration}\right) \tag{5.19}$$

5.1.2 Simulation Results Analysis and Discussion

Two simulations have been conducted in this study. One is the drilling case with the DOD and the other is without the DOD. Other than that, all the simulation conditions are the same. The interest is to compare the results from those two simulations. All the parameters used in the simulations with the single rigid body model are listed in Table 5.1.

Firstly, the two different natural frequencies are calculated with the given parameters. When the drill bit has no contact to the bottom, the natural frequency is 6 Hz. It is 469 Hz for the case of contact. There is quite big difference in the natural frequency between the two cases. However, the given excitation frequency is 18 Hz, quite far

Table 5.1: Parameters used in Dynamic Simulations

Drill Pipe	
Unit Weight W_p	$292N/m$
Length L_p	$2000m$
Cross-sectional Area A_{cross}	$3539\ mm^2$
Elasticity Modulus E_s	$206.8GPa$
Drill Collar	
Length L_c	$60m$
Elasticity Modulus E_c	$206.8\ GPa$
Unit Weight W_c	$1720N/m$
Outer Diameter D_{co}	$177.8mm$
Inner Diameter D_{ci}	$57.2mm$
Rock Properties	
Shear Modulus G_r	$3.65\ GPa$
Poisson's Ratio ν_r	0.37
Density ρ_r	$2100Kg/m^3$
Constants in Bit-rock Interaction Model	
a_1	$3.429 \times 10^{-3} m/s$
a_2	$5.672 \times 10^{-8} m/(Ns)$
a_3	$1.374 \times 10^{-4} m/rd$
Bit factor n_b	1
Constants in Rayleigh Damping	
μ	0.01
λ	0.001
Other	
Drilling Fluid Density ρ_{mud}	$1500Kg/m^3$
Hook load proportionality N	0.5
Pressure Pulsation Acting Area A_p	$7100mm^2$
Foundation Radius r_0	$0.1m$

from both natural frequencies. Therefore, resonance will not occur.

The first simulation is conducted without the external vibration force excitation from the DOD. The BHA is only subjected to the hook load and WOB. Also, in this case, the well bore bottom is assumed as flat surface. Therefore, when the dynamic system becomes stable, it will be only subjected to a constant axial force. Hence, both the BHA displacement and WOB will be stable. With those loads, the bit displacement is around 18 μm and the WOB is about 41.6 KN. Figure 5.6 and Figure 5.3 shows the plots of the BHA displacement and WOB versus time.

Figure 5.2: Displacement Profile When Drilling without the DOD on Flat Surface
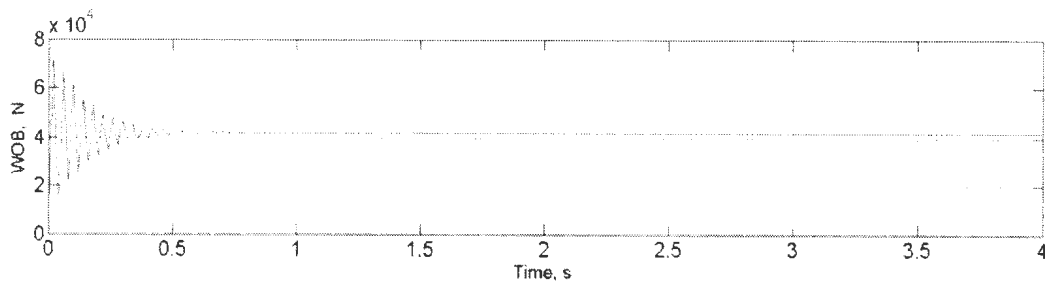
Figure 5.3: Weight on Bit Profile When Drilling without the DOD on Flat Surface

However, when setting the surface elevation as sinusoidal function with 1 mm amplitude, the case will be quite different. Figure 5.4 and Figure 5.5 show the bit displacement and WOB plots in this case. During some time periods, negative displacement appears and WOB becomes zero. This means the bit is off bottom which

represents bit-bounce. Bit-bounce is not welcome since it may cause equipment failures and damage to drill string components. To avoid or alleviate this consequence, WOB needs to be largely increased. However, for the simplicity of the research, the bottom surface is assumed flat surface in the following simulations.
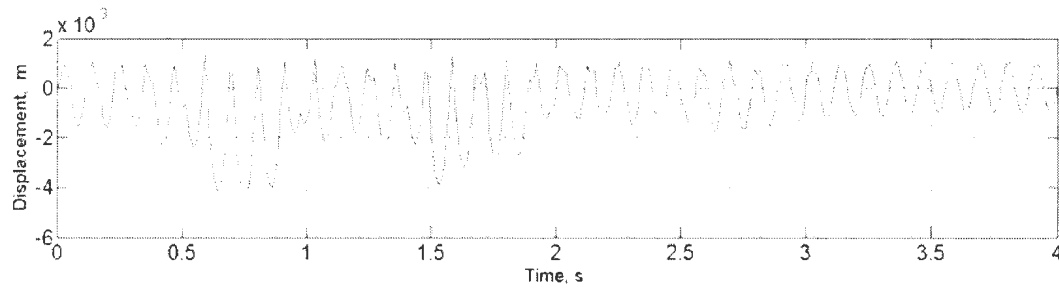
Figure 5.4: Displacement Profile When Drilling without the DOD on Non-flat Surface
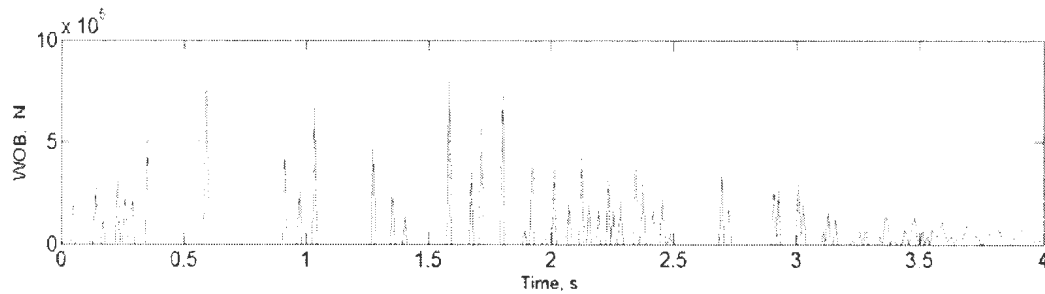
Figure 5.5: Weight on Bit Profile When Drilling without the DOD on Non-flat Surface

Figure 5.2 is the BHA displacement profile of the drilling case with DOD. The displacement vibrates around the mean value of 20 μm which is a small increase compared to 18 μm in Figure 5.6. Also, Figure 5.3 and Figure 5.7 is the comparison on WOB without/with DOD. As mentioned before, the WOB is 41.6 KN when no DOD is involved while it increases to 47.2 KN when the DOD is contained. Since the ROP is proportionally related to WOB and rotating speed of the system (see Equation 5.12), the ROP is increased from 79 ft/hr to 83 ft/hr.
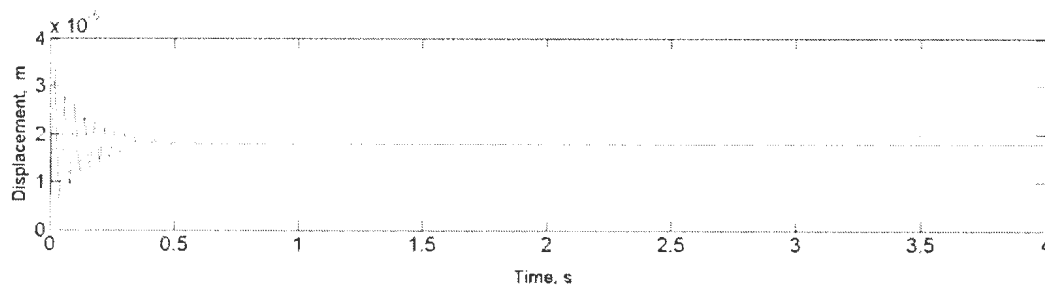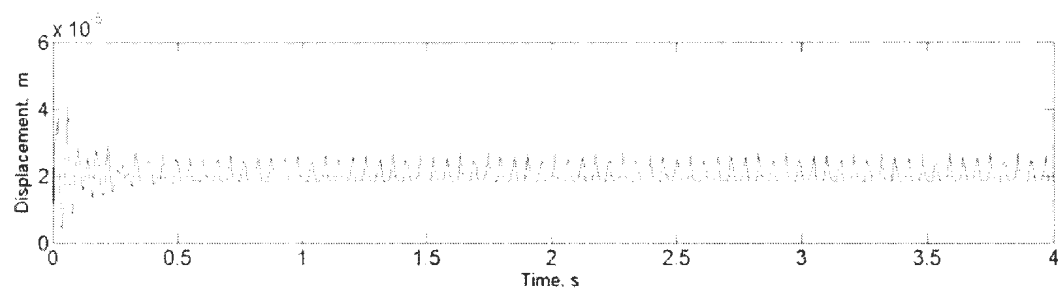
Figure 5.6: BHA Displacement Profile When Drilling with the DOD on Flat Surface
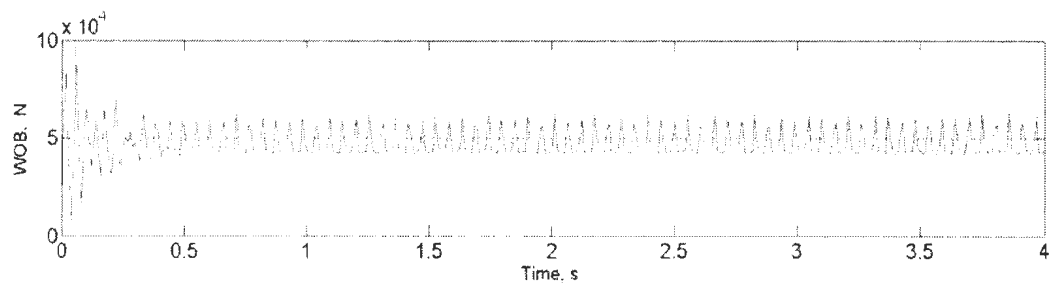
Figure 5.7: Weight on Bit Profile When Drilling with the DOD on Flat Surface

5.2   Simulation with Finite Element Model

5.2.1   Model Introduction

In this section, the finite element model of BHA is introduced and it is employed in the simulations. Figure 5.8 shows the essential components and the geometry of the drill rig. The power system is a rotary table which is driven by an armature controlled DC motor with the transmission by a gearbox[4]. Figure 5.9 schematically shows the FEA model of the BHA. The whole BHA is divided into 30 elements with 31 nodes in total. Each node has two DOF: axial translation and torsional rotation. The bit-rock interaction is simulated as a simple spring-dashpot system with proper system parameters which is the same as that in the previous single rigid body model.
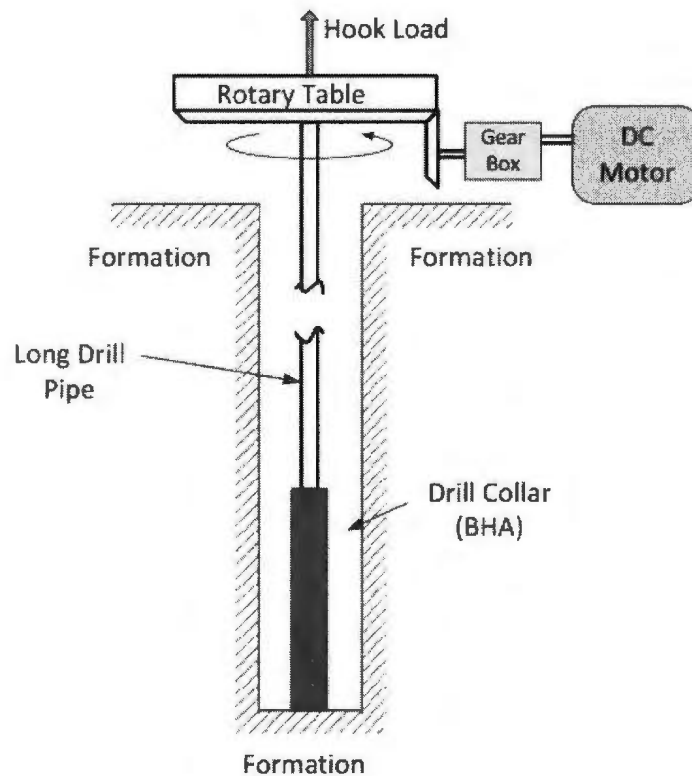
Figure 5.8: General Configuration of the Drill Rig System
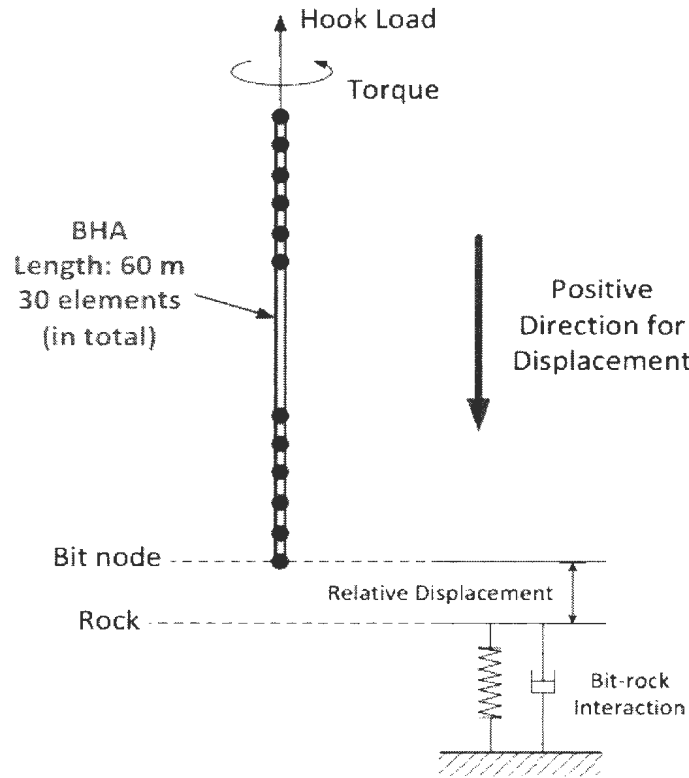
Figure 5.9: Finite Element Model of the Dynamic BHA System

The governing equations of the BHA system are shown as below.

$$M_A \left[\ddot{Z}\right] + C_A \left[\dot{Z}\right] + K_A \left[Z\right] = F_A(Z, \phi) \tag{5.20}$$

$$J_T \left[\ddot{\phi}\right] + C_T \left[\dot{\phi}\right] + K_T \left[\phi\right] = T(Z, \phi) \tag{5.21}$$

In Equation 5.20, M_A, C_A, and K_A are the mass, damping, and stiffness matrices of the system, respectively, $[Z]$ is the axial displacement matrix, F_A represents the overall excitation force in axial direction, which includes the gravity of the BHA, the buoyancy force from the drilling mud, hook load, and WOB. The vibration force is applied to the system in some cases. In Equation 5.21, J_T, K_T and C_T are the rotary

inertia, torsional stiffness, and torsional damping matrices of this dynamic system. $[\phi]$ is the rotation matrix and T represents the resulting torque the system is subjected to. In this case, the overall torque only includes the torque from power system and torque on bit (TOB). The two excitations F_A and T are coupled together in this case and they are introduced later in this section. For simplicity, the two equations are compacted into one which is shown as below.

$$M\left[\ddot{X}\right] + C\left[\dot{X}\right] + K\left[X\right] = F \tag{5.22}$$

where M, C, K, and F are the mass, damping, stiffness, and excitation matrices for BHA elements.

When developing the stiffness matrix of the BHA model using finite element method (FEM), Euler-Bernoulli beam theory is employed. This beam theory assumes linear, small-displacements which means plane section will remain plane during deformation. However, it neglects the shear contributions which are included in the Timonshenko beam theory. Basically, there are standard finite element methods for the derivation of stiffness matrix. The methods are illustrated by Przemieniecki[50], Rao[51], and others.

For each BHA element in this model, linear shape functions are used for torsional and axial strain and this will lead to constant axial load and torque. The element stiffness matrix is 4 by 4 in size with two nodes per element and 2 DOF per node. Figure 5.10 shows the Euler-Bernoulli linear beam element. The stiffness and mass matrices of any BHA element are introduced as below[52].
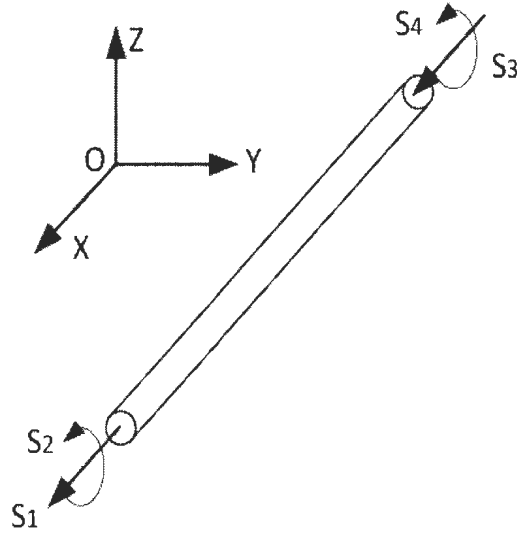
Figure 5.10: Three Dimensional Bernoulli Linear Beam Element with Two DOF at Each End

$$K = \begin{bmatrix} \frac{E_c A}{l} & 0 & -\frac{E_c A}{l} & 0 \\ 0 & \frac{G_c J}{l} & 0 & -\frac{G_c J}{l} \\ -\frac{E_c A}{l} & 0 & \frac{E_c A}{l} & 0 \\ 0 & -\frac{G_c J}{l} & 0 & \frac{G_c J}{l} \end{bmatrix} \tag{5.23}$$

$$M = \frac{W_c l}{g} \begin{bmatrix} \frac{1}{3} & 0 & \frac{1}{6} & 0 \\ 0 & \frac{J}{3A} & 0 & \frac{J}{6A} \\ \frac{1}{6} & 0 & \frac{1}{3} & 0 \\ 0 & \frac{J}{6A} & 0 & \frac{J}{3A} \end{bmatrix} \tag{5.24}$$

where l is the element length in the model. E_c and G_c are the Young's modulus and shear modulus of the drill collar. W_c refers to the drill collar unit weight, g is the gravity acceleration, and J is the moment of inertia of each drill collar element. A is

the cross-sectional area of the drill collar which is calculated from its outer diameter D_{co} and inner diameter D_{ci} as below.

$$A = \pi \frac{D_{co}^2 - D_{ci}^2}{4} \tag{5.25}$$

Rayleigh Damping is employed in this study as below.

$$C = \mu M + \lambda K \tag{5.26}$$

where μ is the mass proportional Rayleigh damping coefficient, λ is the stiffness proportional Rayleigh damping coefficient. As mentioned before, though the tuning of μ and λ is important to the damping parameter, the stable response of the system will not be affected. The reason is that randomness is not considered in this BHA system.

5.2.1.1   Bit-rock Interaction

As mentioned before, the bit-rock interaction is modeled as a spring-dashpot system. However in this research, both torsional and axial motions are included in the model. The WOB is modeled the same with that in the single rigid body model (see Equation 5.7 to Equation 5.11). After the ROP is estimated with Equation 5.12, the TOB is derived by the following equation which was also originally developed by Tucker and Wang[40].

$$TOB = -\frac{ROP}{\omega_{bit}} a_4 - a_5 \tag{5.27}$$

where a_4 and a_5 are the positive constants in this bit-rock interaction model. Obviously, WOB and TOB are coupled in this model. Therefore, the axial and torsional excitations of the BHA are coupled together.

However, there may be a case when the bit rotation stops. For example, stick-slip may occur in drilling. If so, there is a singularity for the TOB calculation in Equation 5.15 since ω_{bit} is the denominator. To avoid this situation, a regularization function is introduced. This function will assure even when the drill bit is not rotating, the torque on bit is still continuous. Figure 5.11 is the plot and Equation 5.28 is the calculation equation of this regularization function. e is the regularization parameter. With this method, the bit-rock interaction model is introduced by Equation 5.29 and Equation 5.30.
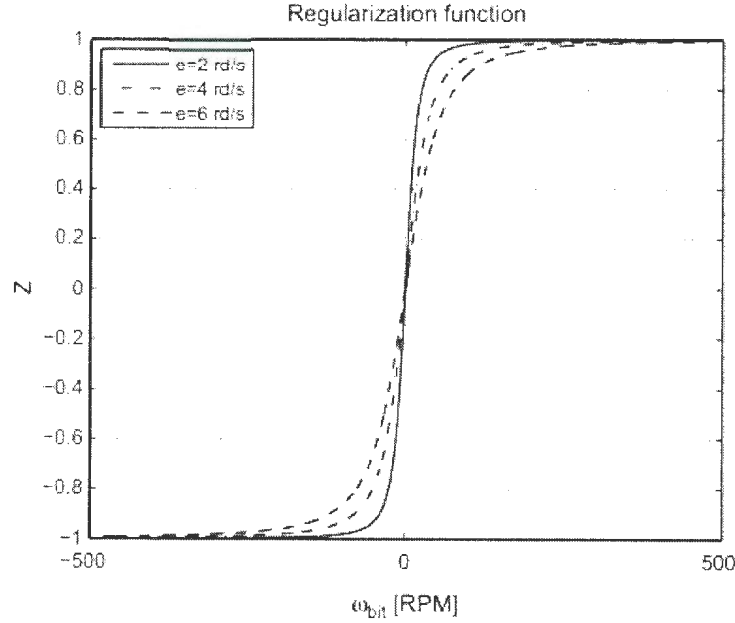
Figure 5.11: Regularization Function[39]

$$Z(\omega_{bit}) = \frac{\omega_{bit}}{\sqrt{(\omega_{bit})^2 + e^2}} \tag{5.28}$$

$$WOB = -\frac{ROP}{a_2 Z(\omega_{bit})^2} + \frac{a_3 \omega_{bit}}{a_2 Z(\omega_{bit})} - \frac{a_1}{a_2} \tag{5.29}$$

$$TOB = -\frac{ROPa_4 Z(\omega_{bit})^2}{\omega_{bit}} - a_5 Z(\omega_{bit}) \tag{5.30}$$

Since the bit-rock interaction model in the FEM model and the previous single rigid body model are similar, there are also two different series of natural frequencies of the system: contact and non-contact cases. The frequencies will be calculated and discussed in this chaper later.

5.2.1.2 Overall Axial Excitations

The buoyancy factor is accounted in the gravity in the same way as that in the single rigid body model. In this finite element model, the hook load on the BHA is assumed as a constant force as well. The assumption is also the same as that in the previous model. Equation 5.16, Equation 5.17, and Equation 5.18 show the calculations for buoyancy factor f_{BF} and hook load F_h, and the external vibration force $F_{vibration}$ from the DOD. The hook load is applied on the first node of the BHA model while the WOB is applied on the last node of the BHA. The external vibration force generated by the DOD is applied to different nodes in order to investigate the effect of loading. The overall axial excitation force for this system is summarised as below.

$$F_A = G - WOB - F_h \left(+F_{vibration}\right) \tag{5.31}$$

5.2.1.3 Overall Torsional Excitations

As mentioned before, the torsional excitation of this system only includes the torque from power system and TOB. Yigit and Chritoforou[4] introduced a method to model the DC motor in operation. In this drilling system, the rotary table is driven by the motor through a gearbox. And T_{rt} is the torque given by the rotary table. The long drill pipe above BHA is assumed having no contact with the well bore for simplicity

in this study. Hence, the rotary table torque will be directly transferred to the top of BHA without any loss. Therefore, the resulting torque is computed as

$$T = T_{rt} - TOB \tag{5.32}$$

TOB is derived in Equation 5.30. And T_{rt} is related to the motor armature current I, resistance R_m and inductance L_m, gearbox ratio n, and the motor constant K_m, the input voltage to the motor V_c, and the desired rotary speed ω_d[4]. The following three equations clearly explain the motor dynamics and the torque generated by the rotary table.

$$L_m \dot{I} + R_m I + K_m n \dot{\phi}_{rt} = V_c \tag{5.33}$$

$$V_c = K_m n w_d \tag{5.34}$$

$$T_{rb} = K_m n I \tag{5.35}$$

5.2.1.4 Calculation of Stress Distribution

When using finite element method to build the dynamic model, the stress distribution along the whole BHA is available. The interest in this model is only axial and torsional motions. Therefore, axial stress σ_{zz} and torsional stress $\sigma_{\phi z}$ for each element are computed[53] as follows. It should be noted that the torsional shear stress $\sigma_{\phi z}$ is for the outer surface of BHA.

$$\sigma_{zz} = E_c \frac{\Delta z}{l} \tag{5.36}$$

$$\sigma_{\phi z} = G_c \frac{D_{co}}{2} \frac{\Delta \phi}{l} \tag{5.37}$$

where E_c and G_c are elasticity and shear modulus of the drill collar, D_{co} is the outer diameter of the drill collar, l is the element length, Δz and $\Delta \phi$ are the axial displacement difference and torsional rotation difference between the two ends of each element.

5.2.2 Central Differential Method for Multi-DOF System

To solve the differential governing equations of motion for this multi-DOF system, a numerical method must be used. So far, several numerical approaches are available for the solution of vibration problems, including Finite Difference Method, Runge-Kutta method. Newmark method, etc[54]. In this case. the Finite Difference Method is employed. Basically, the main idea of this method is to use approximations to derivatives. At last, the governing equations and associated boundary conditions can be replaced by the corresponding difference equations. There are three different types of formulations for this method: the forward, backward. and central difference formulas. For this research, the central difference formulas are considered since they are most accurate[54].

In the finite difference method, the solution domain is replaced by a finite number of points which are called grid points. Normally, these points are equally spaced along the coordinates (see Figure 5.12). The detailed steps are explained as below.

Using Taylor's series expansion, the grid point i can be expressed with z_{i+1} and z_{i-1} as

$$z_{i+1} = z_i + h\dot{z} + \frac{h^2}{2}\ddot{z} + ... \tag{5.38}$$

$$z_{i-1} = z_i + h\dot{z} - \frac{h^2}{2}\ddot{z} + ... \tag{5.39}$$

Next, the central difference formulas for the velocity and acceleration vectors at time
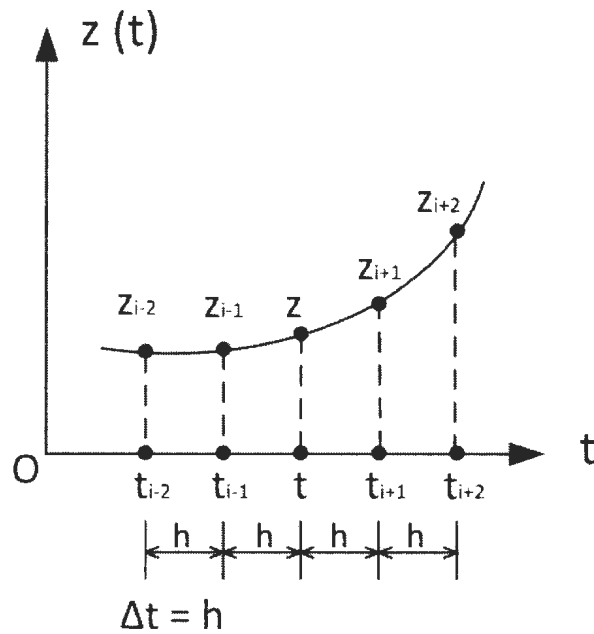
Figure 5.12: Grid Points in Central Difference Method

$t_i = i\Delta t = ih$ are given by the following equations.

$$\dot{z}_i = \frac{1}{2h}(z_{i+1} - z_{i-1})$$
(5.40)

$$\ddot{z}_i = \frac{1}{h^2}(z_{i+1} - 2z_i + z_{i-1})$$
(5.41)

Afterwards, Equation 5.20 at time t_i can be written as

$$M\frac{1}{h^2}(z_{i+1} - 2z_i + z_{i-1}) + C\frac{1}{2h}(z_{i+1} - z_{i-1}) + Kz_i = F_i$$
(5.42)

The above equation can be rearranged to obtain

$$(M\frac{1}{h^2} + C\frac{1}{2h})z_{i+1} = F_i - (K - M\frac{1}{h^2})z_i - (M\frac{1}{h^2} - C\frac{1}{2h})z_{i-1}$$
(5.43)

Once z_i and z_{i-1} are known, the solution for z_{i+1} is available. For the initial condition, z_0 and $\dot{z}_0$ are usually known. However, $\ddot{z}_0$ and z_{-1} can be computed from

$$\ddot{z}_0 = \frac{F_0 - C z_0 - K z_0}{M} \qquad (5.44)$$

$$z_{-1} = z_0 - h\dot{z}_0 + \frac{h^2}{2}\ddot{z}_0 \qquad (5.45)$$

Also, to obtain a satisfactory solution, time step h should be smaller than a critical time step Δt_{cri}. Otherwise, the method will become unstable[54].

$$h < \Delta t_{cri} \qquad (5.46)$$

$$\Delta t_{cri} = \frac{\tau_n}{\pi} \qquad (5.47)$$

where τ_n is the smallest period of the multi-degree-of-freedom system.

5.2.3 Simulation Results Analysis and Discussion

Like the simulations with the single rigid body model, comparative simulations have also been conducted with this finite element model. The goal is to investigate the performance difference from the cases with and without the DOD. Most of the parameters used in the simulations with this finite element model are the same as those for single rigid body model. These parameters have been previously given in Table 5.1, and Table 5.2 lists all the other parameters used in these simulations.

As mentioned before, two different series of natural frequencies of the system are calculated. In the non-contact case, the first five order of non-zero natural frequencies(either axial or torsional) are 166, 268, 333, 501, and 538 Hz. And for the contact case, they are 130, 166, 333, 390, and 501 Hz. The given freqeucy of the external

excitation is 18 Hz, which is not close to these natural frequencies at all. So, there is little possibility of the occurrence of resonance.

When drilling without the DOD, the BHA system is only subjected to a constant axial force and a torsional torque. As a result, the WOB, TOB, and stresses inside the BHA will finally be constants too. However, for the case in which DOD is employed, external vibration force is applied to the first node of the dynamic BHA model. Therefore, the WOB, TOB, and the stresses will oscillate periodically once the system reaches stable state. Finally, the average values are used to compare with the constants from the former simulation case.

Table 5.2: Additional Parameters Used in Dynamic Simulations

Drill Collar	
Total Length L	60 m
Element Length l	2 m
Shear Modulus G_c	79.5 GPa
Moment Inertia J	97012921 mm^4
Constants in Bit-rock Interaction Model	
a_4	$9.537 \times 10^6 Nrd$
a_5	$1.475 \times 10^3 Nm$
Parameters for DC Motor	
Motor inductance L_m	0.005 H
Armature resistance R_m	0.01 Ω
Motor inductance K_m	6 Vs
Gear ratio of the gearbox n	7.2
Other	
Regularization Coefficient e	2 rd/s
DOD Pulsation Rate ω_d	18Hz

The first simulation result for comparison is WOB. Figure 5.13 shows the WOB result from the non-DOD case while Figure 5.14 is the WOB profile when the DOD is applied to the BHA. When the BHA system becomes stable in both cases, the average WOBs from drilling with and without the DOD are 31.9 KN and 37.4 KN respectively. This is a 17.5% increase in WOB with the application of the DOD. ROP can then be calculated with Equation 5.12. It turns out that the ROP is improved from 72.5 ft/hr to 76.3 ft/hr.
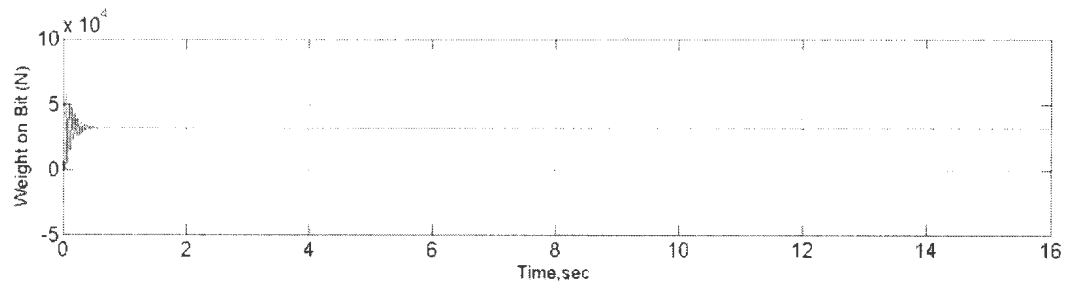
Figure 5.13: WOB Result When Drilling without the DOD
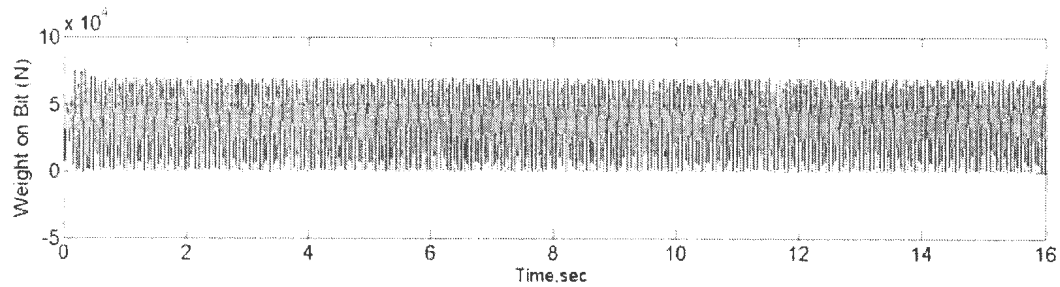
Figure 5.14: WOB Result When Drilling with the DOD

The second parameter for comparison is the TOB. Figure 5.15 and Figure 5.16 show the TOB results from the simulations with and without the DOD. As shown in the figures, the average TOB is increased from 2510 N·m to 2563 N·m when applying the DOD to drilling. The torque increase is not huge; however, it fluctuates a lot when

the DOD employed. This indicates that adding the DOD may cause easier fatigue failure of the BHA components and even the possibility of stick-slip. Therefore, this proves that axial vibration force does influence the torsional motion of the system. And the influence is not small.
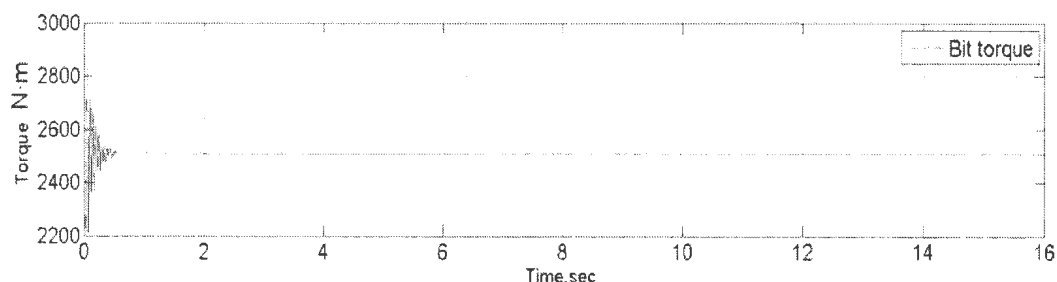
Figure 5.15: TOB Result When Drilling without the DOD
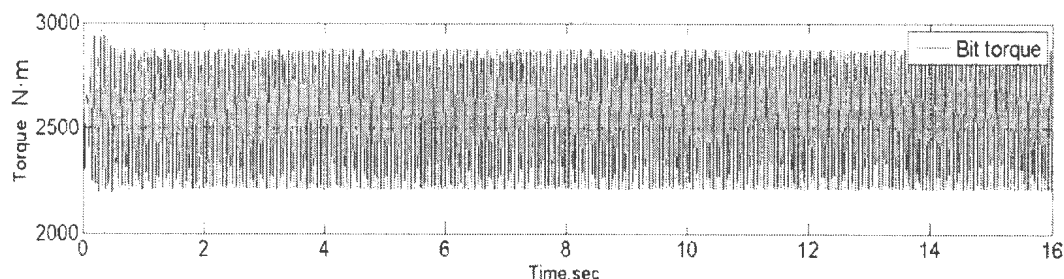
Figure 5.16: TOB Result When Drilling with the DOD

With finite element method, it is feasible to study the stress distribution along the whole BHA. Figure 5.17 and Figure 5.18 show the comparison for the axial stress in the bit element. As shown in the figures, the bit sub is always in compression when drilling without the DOD and the stress is quite stable. However, when using the DOD, the axial stress in the bit element varies a lot. The peak-to-peak variation can be as big as 3.1 MPa. For most of the time in a cycle, the bit stress is negative which means the bit is in compression.

Figure 5.17: Axial Stress Result in the Bottom Element of BHA When Drilling without the DOD
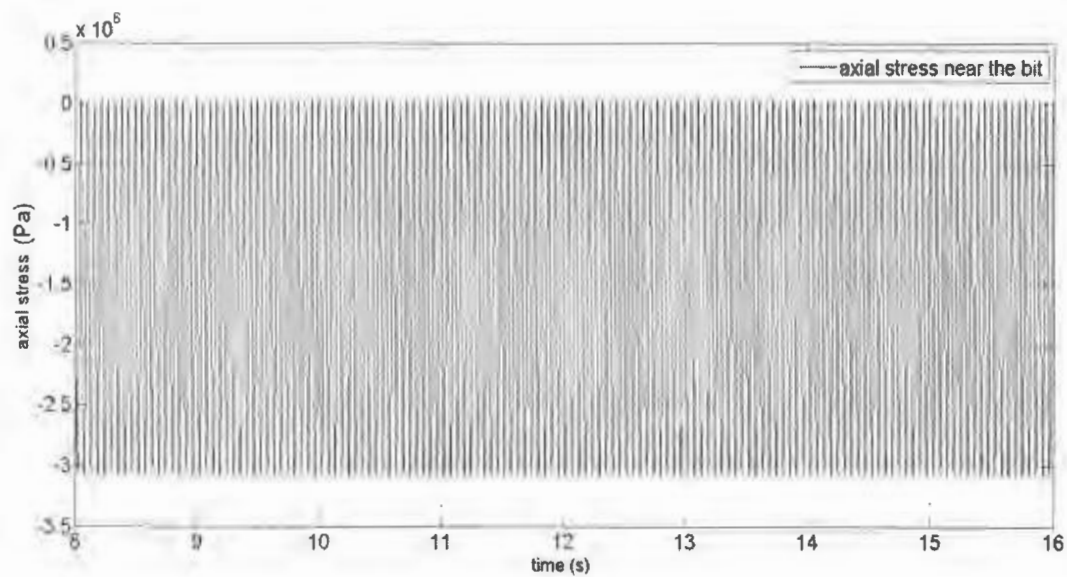
Figure 5.18: Axial Stress Result in the Bottom Element of BHA When Drilling with the DOD

Figure 5.19 and Figure 5.20 compare the axial stress for the top element of the BHA. Both figures mean that this element is in tension. In the non-DOD case, the tensile stress is stable with 2.26 MPa. However, in the case with DOD, the tensile stress is vibrating around the mean value of 1.84 MPa. The amplitude of this stress variation is 0.43 MPa. Hence, the mean tensile stress is decreased when installing the DOD on the top of the BHA.
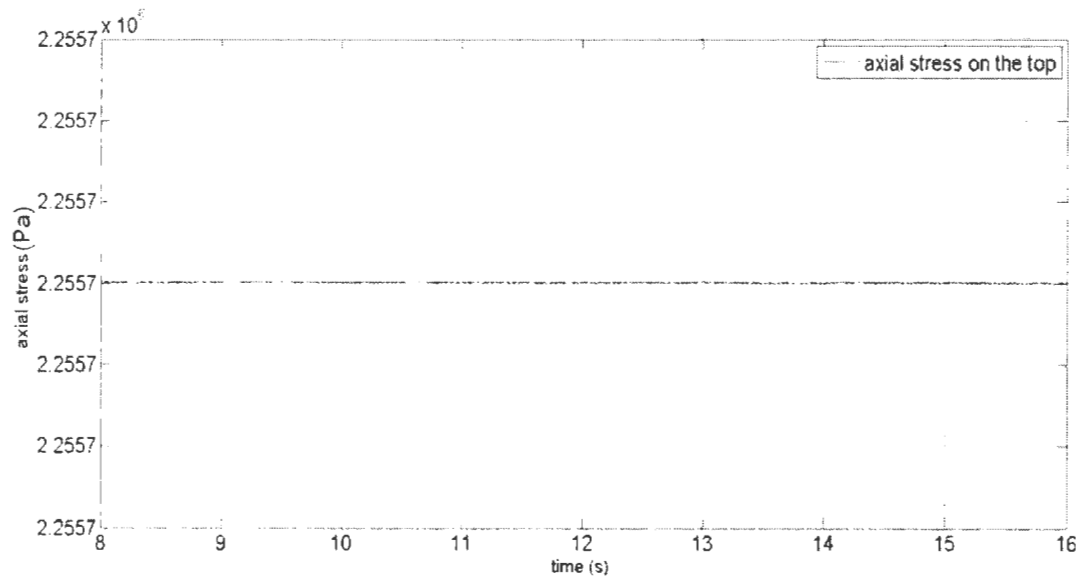
Figure 5.19: Axial Stress Result on the Top of BHA When Drilling without the DOD

Figure 5.21 and Figure 5.22 are the torsional stress profiles for the BHA bottom element when drilling with/without the DOD. In the non-DOD case (see Figure 5.21), the stress is almost stable with the value of 2.3 MPa. However in the case with the DOD, the torsional stress is oscillating around the mean value of 2.36 MPa (see Figure 5.22). The amplitude of this variation is about 0.3 MPa. Figure 5.23 and Figure 5.24 are the torsional stress profiles for the top element when drilling with-/without the DOD. In the non-DOD case (see Figure 5.23), the stress is almost stable with the value of 2.32 MPa. However in the case with the DOD, the torsional stress
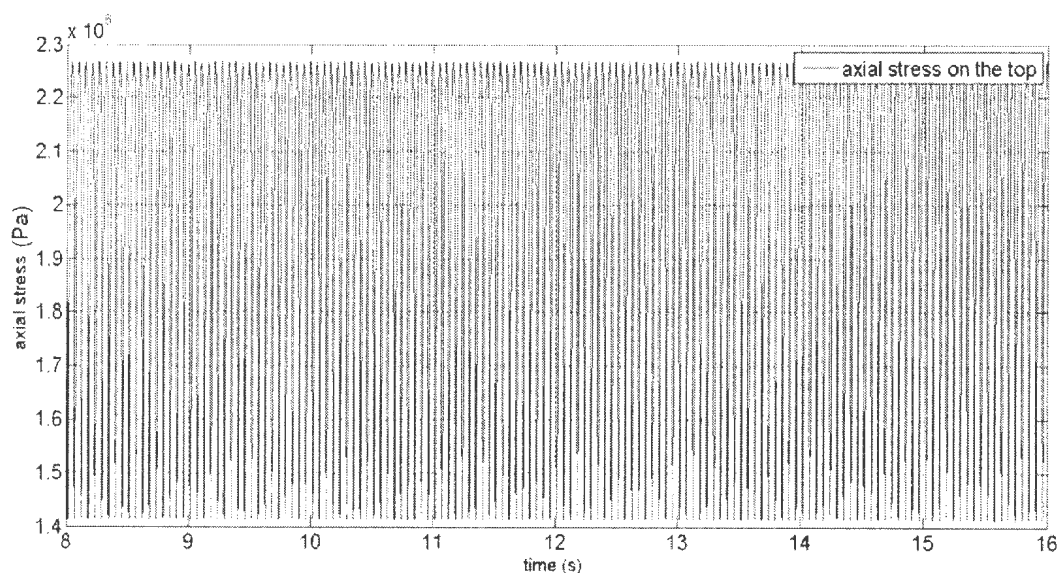
Figure 5.20: Axial Stress Result on the Top of BHA When Drilling With the DOD

is oscillating around the mean value of 2.37 MPa (see Figure 5.24). The amplitude of this variation is about 0.26 MPa. As a result, adding the DOD to the BHA top will increase the mean torsional stress of both the bottom and top element. However, the increase is small. When drilling with the DOD, the stress amplitude of the bottom element is a little bigger than that of the top element. Besides, the stress difference between the top element and the bottom element is small in both cases.

Figure 5.25 and Figure 5.26 show the axial and torsional stress distribution along the whole BHA. In each figure, results from the previous two simulations are plotted for comparison. Figure 5.25 displays how the axial stress varies in different part of BHA. As shown in the figure, from the top element of BHA to bit sub, the axial stress is changing from tension to compression. There is one point which has the axial stress of 0. As mentioned before, this point is called the neutral point. As shown in the figure, this neutral point moves up along the BHA towards surface when the DOD is employed in drilling. This means less part of the BHA is in tension in this case.
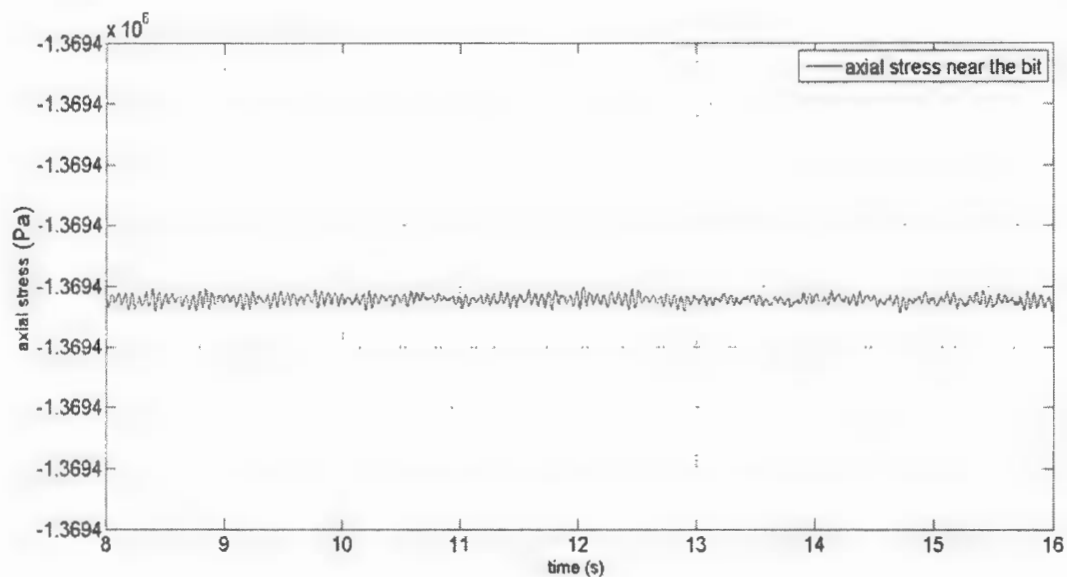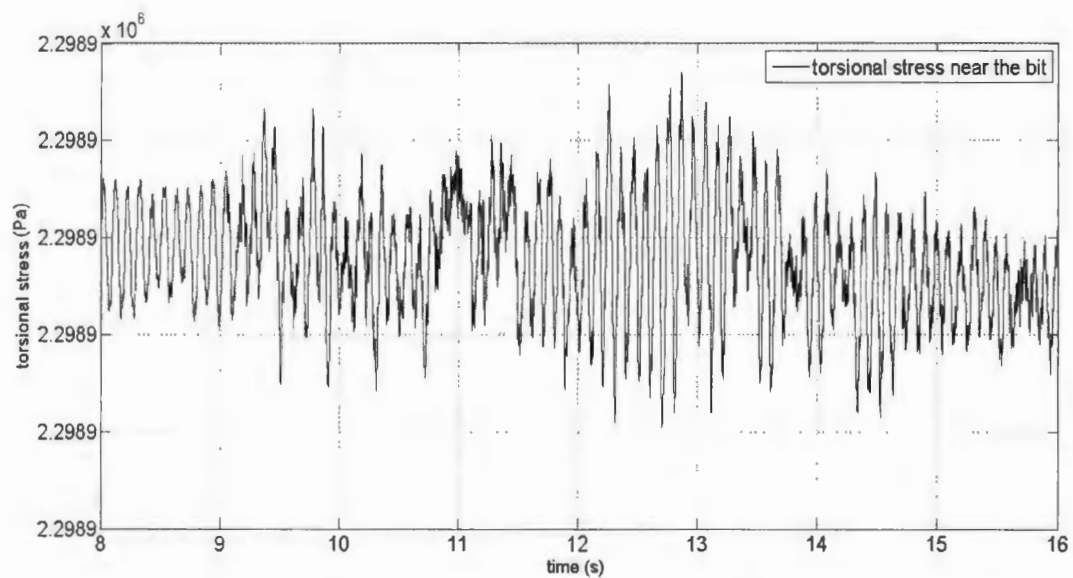
Figure 5.21: Torsional Stress Result in the Bottom Element of BHA When Drilling without the DOD
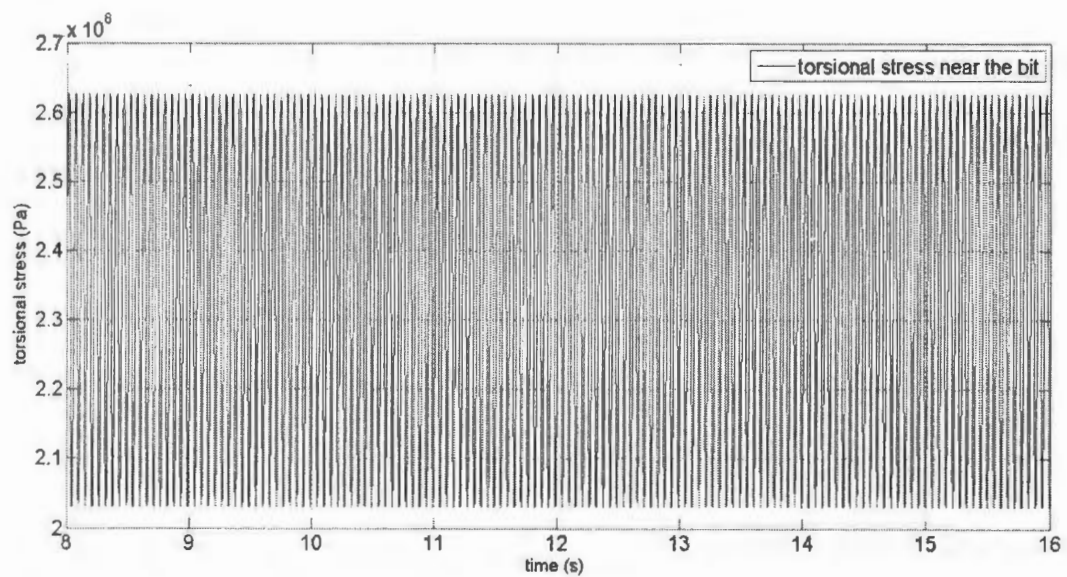
Figure 5.22: Torsional Stress Result in the Bottom Element of BHA When Drilling with the DOD
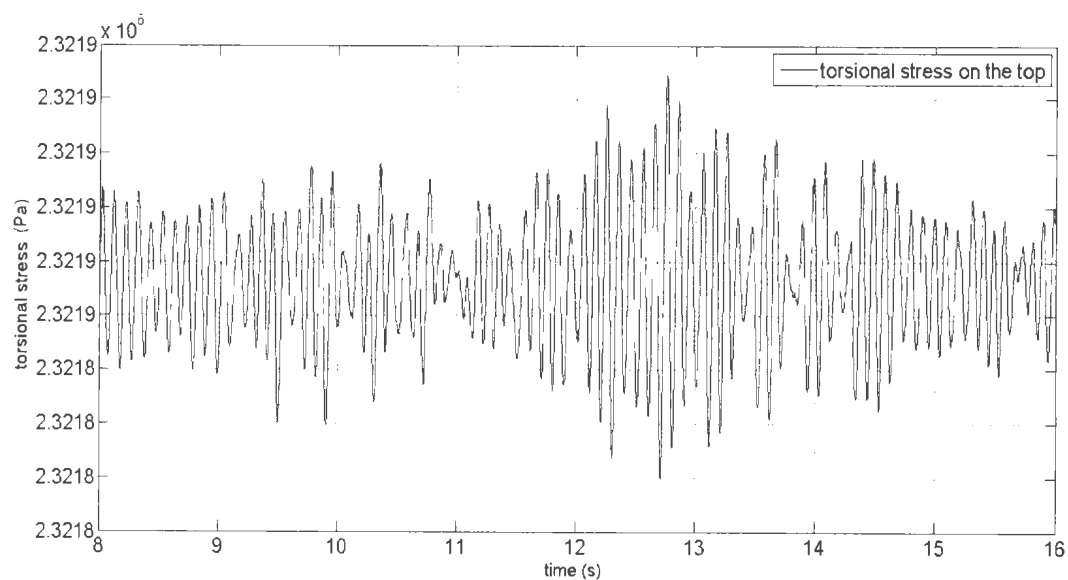
Figure 5.23: Torsional Stress Result in the Top Element of BHA When Drilling without the DOD
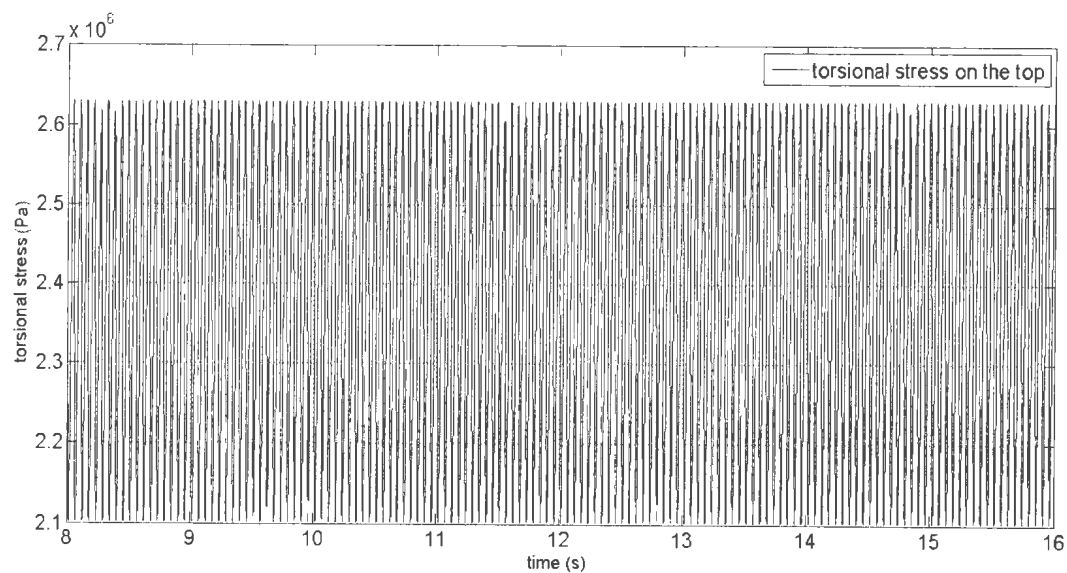
Figure 5.24: Torsional Stress Result in the Top Element of BHA When Drilling with the DOD

Figure 5.26 compares the torsional stress distribution along the BHA. As shown in the figure. in the non-DOD case, the torsional stress is slowly decreasing along the BHA from the top to the bottom. Although the overall trend is still slowly decrease in the case with DOD, the element which has the highest torsional stress is not the top one. However, the torsional stress in each element is increased when the DOD is involved in drilling. Also, the stress increment varies along the BHA. All the stress results obtained will be significantly useful when investigating fatigue failure of the BHA in future studies.
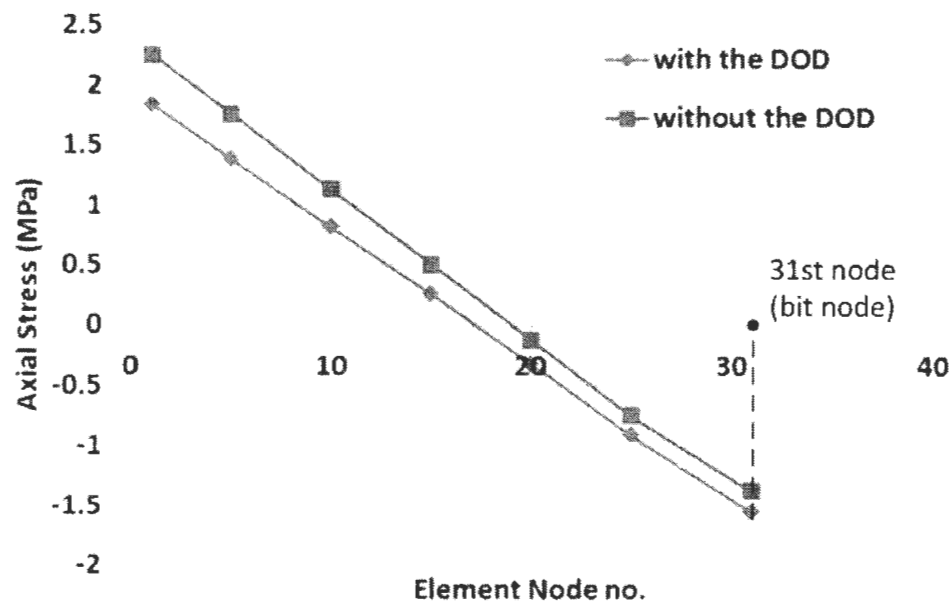
Figure 5.25: Comparison of the Axial Stress Distribution along BHA

5.2.4 Vibration Force Optimization with Finite Element Model

It is suggested from the previous simulation results that external vibration force from the DOD can improve ROP. Most research to date has focused on the influence of vibration forces applied to individual cutter using Distinct Element Models[55, 56].
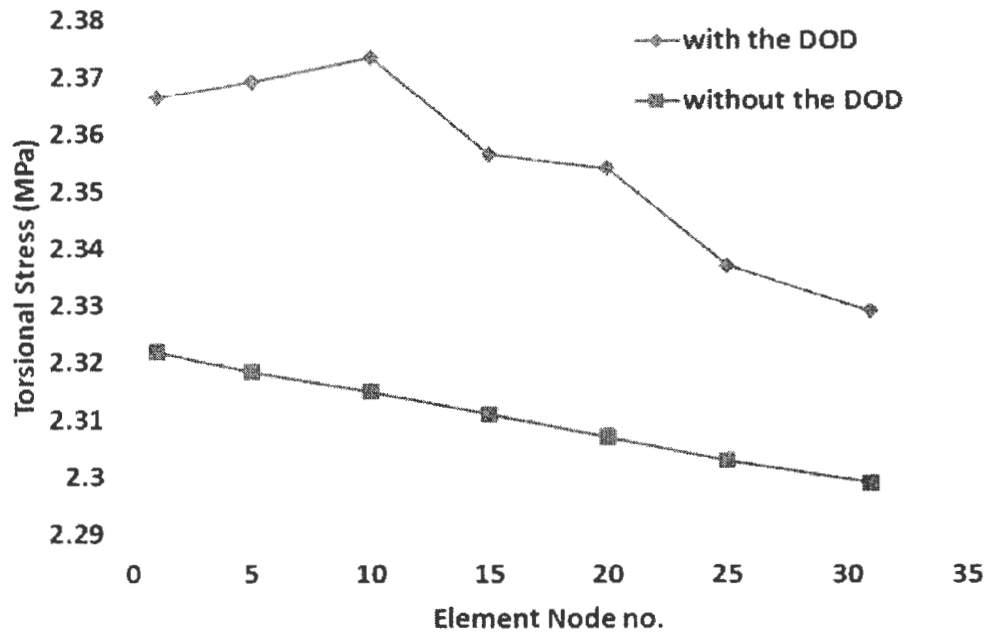
Figure 5.26: Comparison of the Torsional Stress Distribution along BHA

However, this has not been investigated using Finite Element Models of the drill string. For this purpose, a series of FEM simulations are conducted. The vibration force investigated in this research is simply harmonic. There will be variations for all the parameters like mean value F_{mean}, amplitude F_{amp}, and the angular frequency ω_{vib}. Also, the placement of the vibration force on the BHA will be examined too.

$$F_{vibration} = F_{mean} + F_{amp}sin(\omega_{vib}t) \tag{5.48}$$

In the following discussion, only the average WOB and ROP are compared while the TOB is not. The reason is that the variation in TOB is similar to WOB since the TOB is linear to WOB when the rotation speed is not changing (See Equation 5.12). Figure 5.27 schematically shows how average WOB and ROP change while increasing the mean value of the external vibration force. It is shown that both average WOB

and ROP are proportional to F_{mean}. It is noted that when the mean force is increased from 10 KN to 40 KN, the drilling WOB is improved from 42 to 72 KN. As mentioned above, the drilling WOB without vibration force is 37.9 KN. This makes the WOB improvement varies from 10.8% to 90% in this vibration force range. Corresponding to this WOB change, the drilling average ROP increases from 80 to 100 ft/hr (See Equation 5.12). It is an improvement of 9.3% to 37% when the drilling with external vibration force.
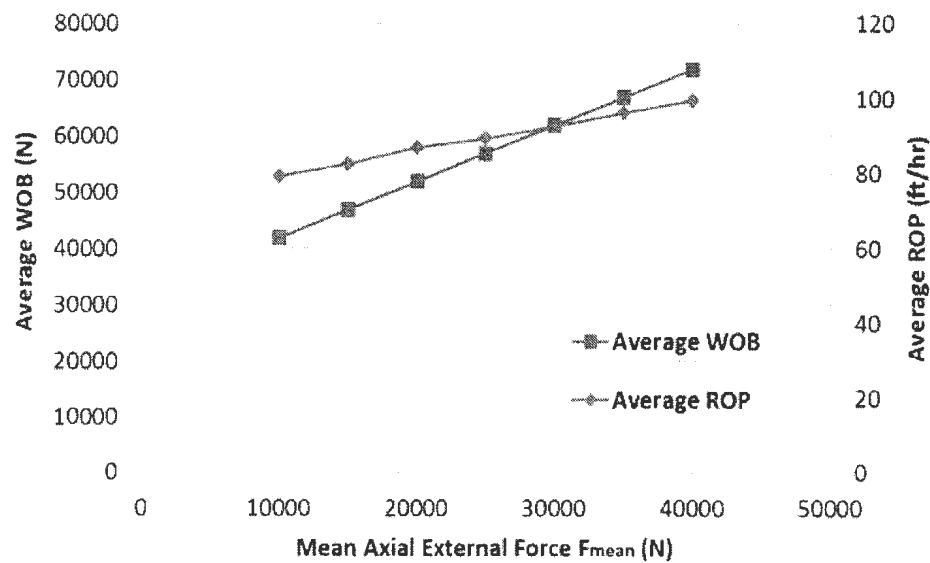
Figure 5.27: Average WOB/ROP vs. Mean Value of External Vibration Force

The amplitude of this external vibration force should also be noticed since there is probability that it may bring some influence to drilling. Figure 5.28 shows the relationship of average WOB and ROP versus the vibration force amplitude. The mean value of the vibration force for this group of simulations is 40 KN. When the force amplitude is increased from 0 KN to 40 KN, the average WOB increment is from 71.87 KN to 80 KN. The corresponding ROP is increased from 99.35 to 99.43 ft/hr. As a result, increasing F_{amp} does improve average WOB and ROP, but the influence

is limited.
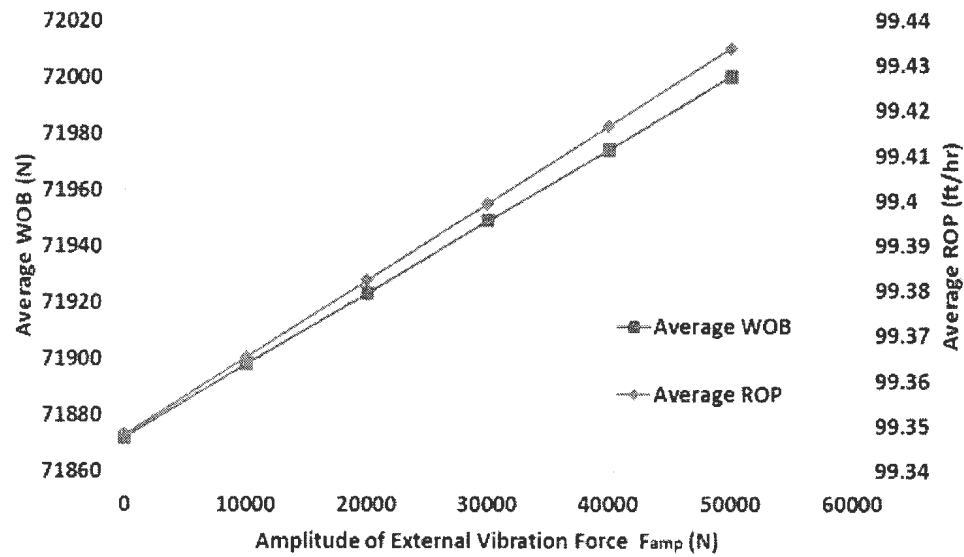
Figure 5.28: Average WOB/ROP vs. Amplitude of External Vibration Force

Angular frequency ω_{vib} is another characteristic of the external vibration force. Its influence on average WOB and ROP is shown in Figure 5.29. It is noted that for a vibration force with certain angular frequency, higher average WOB and ROP are obtained than other frequencies. And this optimised angular frequency is low. However, the difference between the maximum and minimum WOB/ROB is tiny (175N for WOB and 0.1 ft/hr for ROP). Besides, when the angular frequency exceeds 200 rad/s, it has little influence. It is concluded that the angular frequency of the external vibration force has little effect on drilling enhancement.

Where to apply this external vibration force in the BHA may be of great importance. Therefore, this group of simulations are focused on this problem. Seven different locations are set in the simulations: 1st, 5th, 10th, 15th, 20th, 25th, and 31st node of the BHA model. The first node is the BHA top node and the 31st node is the bit node. As shown in Figure 5.30, there is some increase in both average WOB and
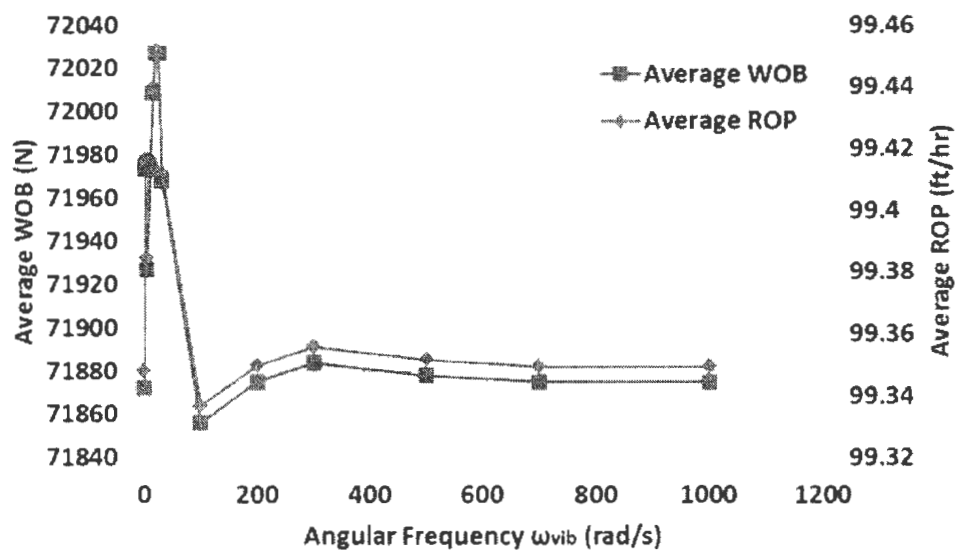
Figure 5.29: Average WOB/ROP vs. Angular Frequency of External Vibration Force in BHA

ROP when the force placement is moved from top BHA to drill bit. However, the improvements are small and can be considered negligible. Hence, the location of the external force on the BHA barely has any effect on drilling enhancement.

In summary, this chapter introduces two different dynamic models for the BHA. They are single rigid body model and finite element model. Comparative simulations are conducted for each model. The comparison is between the simulations whether the DOD is employed in the BHA. Additional simulations are conducted with the FEA model to investigate how various external vibration forces affects drilling enhancement. The results of the simulations focus on average WOB, TOB, and ROP, etc., and not on the dynamic peak-to-peak variations in these quantities. As a result, no conclusions can be made regarding the influence of dynamic vibration on drilling performance. This can be addressed in future research and in fact it is the focus of other activities in the Advanced Drilling Group at Memorial University.
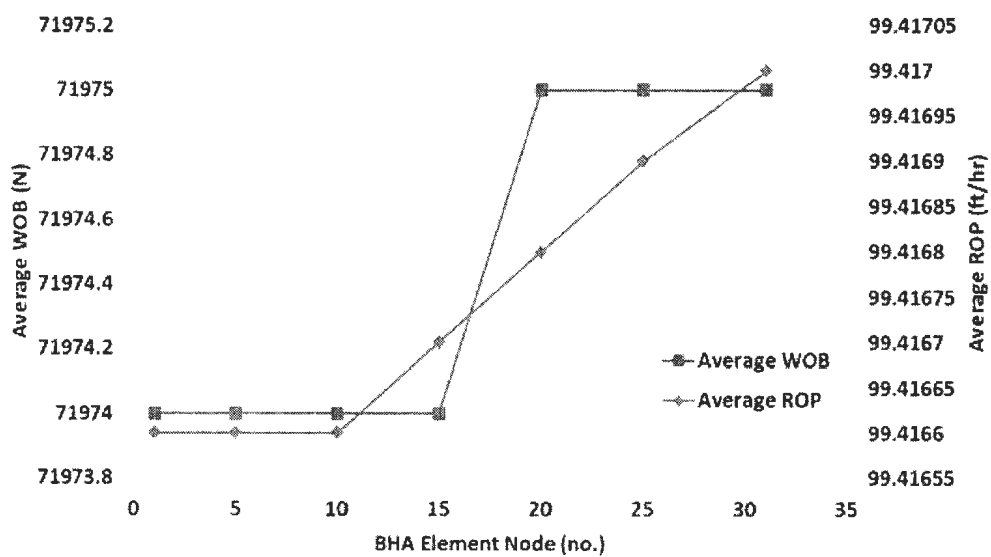
Figure 5.30: Average WOB/ROP vs. Placement of External Vibration Force in BHA

Chapter 6

Conclusion and Discussion

6.1 Conclusions

This thesis introduced a vibration assisted rotary drilling (VARD) tool called Down-
hole Oscillating Device (DOD) which is designed to enhance drilling. A 3D model
was built based on its working mechanism. Then, CFD simulation is conducted to
study the output from the DOD. Next, those simulation results are treated as the
excitations for the BHA model in the dynamic simulations. The results from the
dynamic simulations suggest how the DOD affects drilling.

The CFD simulations show that the DOD could generate pressure pulsations. Also, it
is revealed that the drilling fluid significantly affects the pressure pulsations generated
by the DOD. When drilling with water, the amplitude of pressure pulse is around 2.6
MPa. However, with drilling mud of higher density and higher viscosity, the pressure
pulse amplitude increases. Relatively, the density affects the pressure pulse amplitude
more significantly than the viscosity. The simulation results are obtained with the
simulation parameters from Table 4.2. The CFD simulations set a good example
for an easy way to research the relative simple drilling tool's performance. In the

research, the influence from drilling mud properties can be thoughly studied. Thus, CFD simulation is a good way to develop the most suitable drilling fluid property for any particular drilling cases.

The results from dynamic simulations are based on the parameters from Table 5.1 and Table 5.2. The simulation with the single rigid body model shows the increase in both WOB and ROP when applying the DOD to the BHA. With that 2.6 MPa pressure pulse, the WOB is increased from 41.6 KN to 47.2 KN. Consequently, the ROP also has an increase from 79 ft/hr to 83 ft/hr. However, the single rigid body model is based on the assumptions that the long drill pipe is treated as a spring-dashpot connection. Therefore, this model is limited to the cases with really simple conditions. And this model is only used to develop the rough estimation of the external force performance. For more accurate investigation, advanced model needs to be developed.

The first two simulations with the finite element model are to evaluate the DOD's performance too. It is indicated that the average WOBs in drilling with and without the DOD are 31.9 KN and 37.4 KN respectively. This is a 17.5% of WOB increase with the application of the DOD. ROP can then be calculated based on a proper model. It turns out that ROP is improved from 72.5 ft/hr to 76.3 ft/hr. Therefore, the simulation results with different dynamic models quite agree with each other. The increments in ROP are very close. The stress distributions in both axial and torsional directions are displayed in the thesis. All the results can be applied to future research in VARD tool design optimization and BHA fatigue failure prediction.

Another series of dynamic simulations are conducted with the FEA model. This is for the investigation that how the characteristics of the external vibration force affect the enhancement. The vibration force employed here is harmonic. As a result, when the mean vibration force F_{mean} is increased from 10 KN to 40 KN, the drilling WOB is improved from 42 to 72 KN. Corresponding to this WOB change, the drilling average

ROP is increased from 80 to 100 ft/hr. It is an improvement of 9.3% to 37% when the drilling with external vibration force. Besides, when the force amplitude F_{amp} is increased from 0 KN to 40 KN, the average WOB increment is from 71.87 KN to 80 KN and the corresponding ROP has only 0.1 ft/hr increase. The influence from force amplitude is limited. Besides, the angular frequency of the external vibration force hardly affects drilling enhancement. Finally, although there is some increase in both average WOB and ROP when the force placement is moved from top BHA to drill bit, the improvements are small and can be considered as negligible. As so, external force placement in the BHA barely has any effects on drilling enhancement. Therefore, it is applicable to utilize vibration force with higher mean value and amplitude to improve drilling ROP. However, severe vibration can result in easy fatigue failure, severe bit wear, short bit life, and even BHA components damage. It is essential to find out the balance.

6.2   Future Work

In this research, only the axial and torsional motions are considered in the dynamic models of BHA. However, drilling is a complex process. Axial, torsional, and lateral motions of the BHA are coupled together in the real case. Therefore, proper modifications can be added to both dynamic BHA models in this research work.

When establishing the dynamic model, the whole BHA is treated as a steel pipe. However, the real BHA is comprised of various components. The equipment cannot be simply regarded as steel pipes. Special components like shock subs, MWD tools, motors, turbines, and jars all have unique stiffness properties due to their special configurations. It has become necessary to investigate their unexpected stiffness properties. Mass imbalance should also be accounted in future study. Additionally,

the friction between the drill string and the well-bore and bottom-hole pressure are all the factors which may affect drilling. More precise model will be developed when update the model on those aspects.

Therefore, in the future studies, the full coupled model needs to be developed for the drill string system. All the affecting factors mentioned above should be considered. Besides, the stachastic phenomena in drilling also needs to be appropriately modelled. Those complexities are not considered in this research work. The reason is that this level of complexity is beyond the scope of a Master's project, and omniting it still gives valuable insight into system dynamics, sensitivities, and quantitative trends.

To verify if the results from the simulations are reasonable or not, lab experiments should also be conducted under the same conditions. The comparison between simulation results and experiment data can reveal more about DOD performance. And this is another challenge in future research.

Bibliography

[1] Amorim. D., Hanley, C., Leite Carvalho. D. (2012, April). *BHA Selection and Parameter Definition Using Vibration Prediction Software Leads to Significant Drilling Performance Improvements*. In SPE Latin America and Caribbean Petroleum Engineering Conference.

[2] Berlioz, A., Der Hagopian, J., Dufour, R., & Draoui, E. (1996). *Dynamic behavior of a drill-string: experimental investigation of lateral instabilities*. Journal of vibration and acoustics, 118(3), 292-298.

[3] Christoforou. A. P., & Yigit, A. S. (2003). *Fully coupled vibrations of actively controlled drillstrings*. Journal of Sound and Vibration, 267(5), 1029-1045.

[4] Yigit. A. S., & Christoforou, A. P. (2006). *Stick-slip and bit-bounce interaction in oil-well drillstrings*. Journal of Energy Resources Technology, 128, 268.

[5] Wikipedia. (June 23, 2006). *Drilling rig*. In WIKIPEDIA.

[6] NaturalGas.org. (June 23. 2006). *Rotary Drilling*. In NaturalGas.org.

[7] Azar, J. J., & Samuel, G. R. (2007). *Drilling engineering*. PennWell Books.

[8] Discovery Drilling Funds. (June 23, 2006). *Anatomy of a Land Based Drilling Rig*. In Discovery Drilling Funds.

[9] Discovery Drilling Funds. (June 23, 2006). *Anatomy of a Land Based Drilling Rig - Hoisting System.* In Discovery Drilling Funds.

[10] Discovery Drilling Funds. (June 23, 2006). *Anatomy of a Land Based Drilling Rig - Circulating System.* In Discovery Drilling Funds.

[11] Discovery Drilling Funds. (June 23, 2006). *Anatomy of a Land Based Drilling Rig - Rotating System.* In Discovery Drilling Funds.

[12] Wikipedia. (June 23, 2006). *Kelly drive.* In WIKIPEDIA.

[13] Wikipedia. (June 23, 2006). *Top drive.* In WIKIPEDIA.

[14] Wikipedia. (June 23, 2006). *Blowout (well drilling).* In WIKIPEDIA.

[15] Norris McDonald. (Monday, May 03, 2010). *Offshore Blowout Preventer (BOP): Companies & Equipment. In Center for Environment,* Commerce & Energy.

[16] Barton, S., Baez, F., & Alali, A. (2011, June). *Drilling Performance Improvements in Gas Shale Plays using a Novel Drilling Agitator Device.* In North American Unconventional Gas Conference and Exhibition.

[17] Li. G., Shi, H., Niu, J., Huang, Z., Tian, S., & Song, X. (2010, June). Hydraulic Pulsed Cavitating Jet Assisted Deep Drilling: An Approach To Improve Rate Of Penetration. In International Oil and Gas Conference and Exhibition in China.

[18] Lavrut, E., Kante, A., Rellinger, P., & Gomez, S. R. (2005). U.S. Patent No. 6,970,398. Washington, DC: U.S. Patent and Trademark Office.

[19] Nagib, M., Isu, S., Ugbogu, N. I., & G. Nasr, G. (2011, September). *Modeling of a Down hole Pulsating Device.* In SPE Middle East Oil and Gas Show and Conference.

[20] Ibrahim, G., Drenth, C. L., & Lachance, A. (2011). U.S. Patent No. 7,900,716. Washington, DC: U.S. Patent and Trademark Office.

[21] Rosine, R., Bailey, M., & Blanco, I. (2005, April). *Fluid-Flow Phenomenon in CT Using CFD*. In SPE/ICoTA Coiled Tubing Conference and Exhibition.

[22] Zhou, Y., & Shah, S. (2003, June). *Fluid Flow in Coiled Tubing: CFD Simulation*. In Canadian International Petroleum Conference.

[23] Pereira, F. A. R., Barrozo, M. A. S., & Ataíde, C. H. (2007). CFD predictions of drilling fluid velocity and pressure profiles in laminar helical flow. Brazilian Journal of Chemical Engineering, 24(4), 587-595.

[24] Neto, J. L., Martins, A. L., Neto, A. S., Ataíde, C. H., & Barrozo, M. A. S. (2011). *CFD applied to turbulent flows in concentric and eccentric annuli with inner shaft rotation*. The Canadian Journal of Chemical Engineering, 89(4), 636-646.

[25] Nouri, J. M., & Whitelaw, J. H. (1994). *Flow of Newtonian and non-Newtonian fluids in a concentric annulus with rotation of the inner cylinder*. Journal of Fluids Engineering;(United States), 116(4).

[26] Nouri, J. M., & Whitelaw, J. H. (1997). *Flow of Newtonian and non-Newtonian fluids in an eccentric annulus with rotation of the inner cylinder*. International journal of heat and fluid flow, 18(2). 236-246

[27] Saleh, S. T., & Mitchell, B. J. (1989, April). *Wellbore Drillstring Mechanical and Hydraulic Interaction*. In SPE California Regional Meeting

[28] Cui, H. Q., & Liu, X. S. (1995, November). *Research on helical flow of non-Newtonian fluids in eccentric annuli*. In International Meeting on Petroleum Engineering.

[29] Spanos, P. D., & Payne, M. L. (1992, February). *Advances in dynamic bottomhole assembly modeling and dynamic response determination.* InSPE/IADC Drilling Conference.

[30] Besaisow, A., & Payne, M. (1988). *A study of excitation mechanisms and resonances inducing bottomhole-assembly vibrations.* SPE drilling engineering,3(1), 93-101.

[31] Clayer, F., Vandiver, J. K., & Lee, H. Y. (1990, September). *The effect of surface and downhole boundary conditions on the vibration of drillstrings.* InSPE Annual Technical Conference and Exhibition.

[32] Franca, L. F. (2011). *A bit-rock interaction model for rotary–percussive drilling.*International Journal of Rock Mechanics and Mining Sciences, 48(5), 827-835.

[33] Brennan, M. J., Carrella, A., Waters, T. P., & Lopes Jr, V. (2008). *On the dynamic behaviour of a mass supported by a parallel combination of a spring and an elastically connected damper.* Journal of Sound and Vibration, 309(3), 823-837.

[34] Batako, A. D., Babitsky, V. I., & Halliwell, N. A. (2004). *Modelling of vibro-impact penetration of self-exciting percussive-rotary drill bit.* Journal of sound and vibration, 271(1), 209-225.

[35] Hsieh, T. K. (1962, June). *FOUNDATION VIBRATIONS.* In ICE Proceedings(Vol. 22, No. 2, pp. 211-226). Ice Virtual Library.

[36] Lysmer, J. (1965). *VERTICAL MOTION OF RIGID FOOTINGS.* MICHIGAN UNIV ANN ARBOR COLL OF ENGINEERING.

[37] Gazetas, G. (1983). *Analysis of machine foundation vibrations: state of the art.*International Journal of Soil Dynamics and Earthquake Engineering, 2(1), 2-42.

[38] Richart, F. E., & Whitman, R. V. (1967). *Comparison of footing vibration tests with theory.* Journal of Soil Mechanics & Foundations Div.

[39] Ritto, T. G., Soize, C., & Sampaio, R. (2009). *Non-linear dynamics of a drill-string with uncertain model of the bit-rock interaction.* International Journal of Non-Linear Mechanics, 44(8), 865-876.

[40] Tucker, R. W., & Wang, C. (2003). *Torsional vibration control and cosserat dynamics of a drill-rig assembly.* Meccanica, 38(1), 145-161.

[41] McCarthy, J., Stanes, B., Rebellon, J., Leuenberger, G., Clark, K., Kollker, C., & Grabski, L. (2009, March). *A Step Change in Drilling Efficiency: Quantifying the Effects of Adding an Axial Oscillation Tool Within Challenging Wellbore Environments.* In SPE/IADC Drilling Conference and Exhibition.

[42] Li, H., Butt, S., Munaswamy, K., & Arvani, F. (2010, June). *Experimental Investigation of bit vibration on rotary drilling penetration rate.* In 44th US Rock Mechanics Symposium and 5th US-Canada Rock Mechanics Symposium.

[43] Babatunde, Y., Butt, S., Molgaard, J., & Arvani, F. (2011, June). *Investigation of the Effects of Vibration Frequency On Rotary Drilling Penetration Rate Using Diamond Drag Bit.* In 45th US Rock Mechanics/Geomechanics Symposium.

[44] Wikipedia. (June 23, 2006). *Computational fluid dynamics.* In WIKIPEDIA.

[45] FLOW Science (2012). *FLOW-3D User Manual v10.*

[46] Sovonex Technology. (June 23, 2006). *Drill Pipes.* In Sovonex Technology.

[47] Spanos, P. D., Sengupta, A. K., Cunningham, R. A., & Paslay, P. R. (1995). *Modeling of roller cone bit lift-off dynamics in rotary drilling*. Journal of Energy Resources Technology, 117(3).

[48] Rigs World. (2013). *Oil Drilling Manual-drilling Buoyancy factor using mud weight*. In Rigs World.

[49] Serene Energy. (2013). *Neutral Point. In Serene Energy*.

[50] Przemieniecki, J. S. (1985). *Theory of matrix structural analysis*. Dover Publications

[51] Rao, S. S., & Yap, F. F. (1995). *Mechanical vibrations (Vol. 4)*. Reading, MA: Addison-Wesley.

[52] Chandrupatla, T. R., Belegundu, A. D., Ramesh, T., & Ray, C. (2002). *Introduction to finite elements in engineering (pp. 334-371)*. Englewood Cliffs, NJ: Prentice-Hall.

[53] Rao, S. S., & Kornprobst, P. (2005). *The finite element method in engineering*. Elsevier/Butterworth Heinemann.

[54] Singiresu S. Rao, *Mechanical Vibrations*, 4e Edition, Pearson Education Inc.., ISBN 0-13-120768-7 (2004)

[55] Akbari, B., Butt, S. D., Munaswamy, K., & Arvani, F. (2011, June). *Dynamic Single PDC Cutter Rock Drilling Modeling and Simulations Focusing on Rate of Penetration Using Distinct Element Method*. In 45th US Rock Mechanics/Geomechanics Symposium.

[56] Yousef Gharibiyamchi, (2013) *Evaluation and Characterization of Hydraulic Pulsating Tools and Potential Impedance on Penetration Rock.* Current M.Eng thesis in Advanced Drilling Group at Memorrial University of Newfoundland

Appendix A: 2D Drawing of the Valve Assembly

The following figure presents the 2-Dimensional Drawing of the Valve Assembly Used in CFD Simulation. The unit is in *mm*.
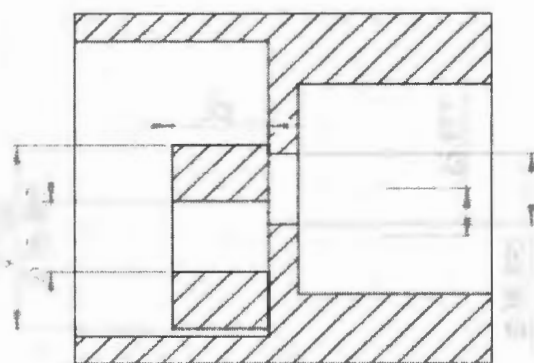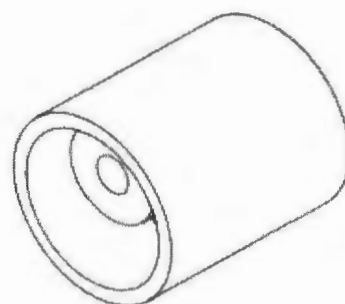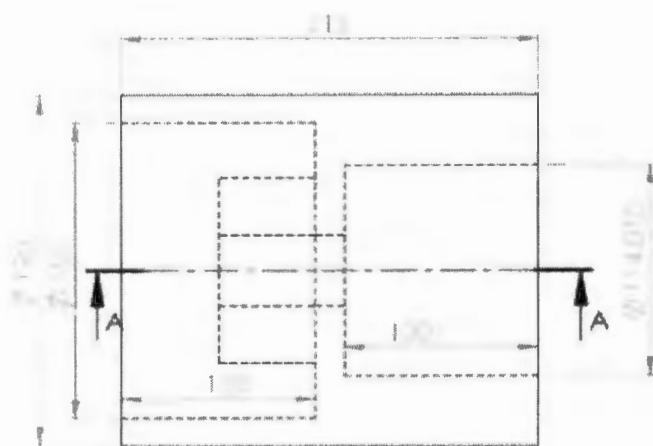
SECTION A-A

Unit: mm

Appendix B: CFD Simulation Results

The following tables show the detailed results of the CFD simulations with four drilling fluids. The fluid properties are presented in Table 4.2. t is the time instant and P represents the pressure magnitude.

Drill mud 1		Drill mud 2	
t(s)	P(0.1 Pa)	t(s)	P(0.1 Pa)
0	0.0	0	0.0
0.004448	0.0	0.004448	0.0
0.008705	0.0	0.009067	0.0
0.012994	0.0	0.013409	0.0
0.017957	0.0	0.017668	0.0
0.022093	0.0	0.021926	0.0
0.027056	474.3	0.026895	488.0
0.031192	124.5	0.031153	127.8
0.035328	-225.3	0.035412	-232.3
0.040292	-555.6	0.040380	-574.8
0.044428	-925.0	0.044638	-952.7

t(s)	P(0.1 Pa)	t(s)	P(0.1 Pa)
0.048820	-1281.7	0.049264	-1326.4
0.053154	-1630.4	0.053161	-1637.0
0.057947	9377.7	0.057493	12274.9
0.062505	4131.0	0.062475	1718.7
0.066592	10973.4	0.066722	8961.0
0.071171	9005.6	0.071470	9076.2
0.075787	9268.1	0.075466	11412.2
0.080022	9709.5	0.080053	10061.2
0.084803	8288.5	0.084749	9398.4
0.088893	11905.5	0.088794	11941.6
0.093325	132320.1	0.093349	200578.6
0.098040	48009.9	0.097677	53521.3
0.102227	50729.8	0.102351	79259.4
0.106754	21330468.0	0.106750	22330606.0
0.111192	32753882.0	0.111201	26360494.0
0.115657	23180060.0	0.115658	22696532.0
0.120083	12825709.0	0.120122	12318322.0
0.124556	2004689.0	0.124573	2148608.5
0.128981	1305394.0	0.129010	1362587.6
0.133461	1249964.2	0.133428	1008390.3
0.137886	1067960.5	0.137907	1132609.8
0.142349	710258.1	0.142333	991390.5
0.146783	1133928.9	0.146765	1190073.9

t(s)	P(0.1 Pa)	t(s)	P(0.1 Pa)
0.151257	1679509.4	0.151279	1683012.9
0.155669	4062138.0	0.155660	4912478.0
0.160143	16795458.0	0.160120	17620946.0
0.164568	25669736.0	0.164570	29241192.0
0.169031	31170176.0	0.169036	27404646.0
0.173487	16511224.0	0.173477	16937400.0
0.177938	5294684.0	0.177908	4066573.0
0.182346	1625611.4	0.182374	1417056.2
0.186802	1114123.2	0.186816	972574.7
0.191306	1224404.1	0.191270	1230326.4
0.195698	890030.3	0.195722	1708982.0
0.200125	893114.8	0.200174	811244.3
0.204605	2341348.8	0.204611	1452348.8
0.209029	2243627.5	0.209055	2356758.0
0.213502	11444407.0	0.213488	13028167.0
0.217958	16815434.0	0.217943	21203880.0
0.222396	30149150.0	0.222389	24233888.0
0.226851	23153898.0	0.226842	21278170.0
0.231276	12070860.0	0.231311	13831501.0
0.235727	2206406.0	0.235759	2006821.0
0.240182	1208878.8	0.240185	1245850.6
0.244625	1095300.2	0.244657	910854.8
0.249058	1145987.1	0.249095	1246821.4

t(s)	P(0.1 Pa)	t(s)	P(0.1 Pa)
0.253568	756698.8	0.253535	689899.7
0.258039	1051244.8	0.257985	1176852.1
0.262397	1963317.6	0.262425	1611459.5
0.266891	3858342.5	0.266881	4861694.5
0.271340	18562894.0	0.271340	17276130.0
0.275767	28575204.0	0.275772	28703766.0
0.280220	31552962.0	0.280232	30504214.0
0.284669	17761220.0	0.284699	17340210.0
0.289124	5030670.5	0.289128	5067009.0
0.293599	1354064.8	0.293569	1644331.5
0.298062	1169941.5	0.298025	956291.7
0.302451	1094141.9	0.302502	1208814.6
0.306891	-81.1	0.306926	1430193.4
0.311340	921935.1	0.311346	768720.0
0.315855	1380977.8	0.315794	1412020.1
0.320252	2414525.2	0.320280	2649419.8
0.324722	12567526.0	0.324715	13128732.0
0.329166	22517060.0	0.329159	21707034.0
0.333605	27564990.0	0.333594	26089062.0
0.338059	19820200.0	0.338054	19597952.0
0.342515	12429680.0	0.342494	12672668.0
0.346951	1964173.4	0.346946	2056236.2
0.351382	1358918.6	0.351420	1292332.0

t(s)	P(0.1 Pa)	t(s)	P(0.1 Pa)
0.355838	1312079.6	0.355863	758606.4
0.360313	1135238.2	0.360307	1044532.6
0.364733	799616.3	0.364758	838349.8
0.369178	1118390.6	0.369145	1056681.0
0.373628	1752452.8	0.373587	1713679.6
0.378059	4216995.5	0.378055	4327378.0
0.382528	17659460.0	0.382529	18645826.0
0.386985	31043348.0	0.386973	31091156.0
0.391414	31341188.0	0.391432	29426440.0
0.395864	15159176.0	0.395887	16582687.0
0.400317	4566826.5	0.400329	4179382.5
0.404779	1541795.5	0.404789	1529153.8
0.409193	1137301.2	0.409253	1242401.5
0.413693	1206256.4	0.413664	839263.1
0.418144	1288945.2	0.418111	721009.3
0.422594	870338.9	0.422565	951354.8
0.427015	1290207.2	0.426995	477655.7
0.431499	2453810.0	0.431484	2357694.8
0.435886	11865950.0	0.435885	13511773.0
0.440345	20940902.0	0.440350	22336348.0
0.444823	27466104.0	0.444821	28816370.0

Drill mud 3		Water	
t(s)	P(0.1 Pa)	t(s)	P(0.1 Pa)
0	0.0	0	0.0
0.004448	0.0	0.004448	0.0
0.009067	0.0	0.009120	0.0
0.013409	0.0	0.013156	0.0
0.017668	0.0	0.017623	0.0
0.021926	0.0	0.022090	0.0
0.026895	665.4	0.026557	169.6
0.031153	174.3	0.031024	126.2
0.035412	-316.8	0.035491	-217.1
0.040380	-783.8	0.039958	-480.6
0.044638	-1299.2	0.044425	-641.3
0.049264	-1808.7	0.049107	-176.1
0.053161	-2232.3	0.053201	5401.5
0.057502	17943.0	0.057549	3847.3
0.062462	2000.7	0.062434	5302.8
0.066928	13426.1	0.066819	6258.0
0.071060	13487.3	0.071321	8731.6
0.075812	13369.8	0.075603	5310.0
0.079911	13703.8	0.080019	8829.3
0.084299	8906.0	0.084667	4763.0
0.088800	16948.9	0.089190	10369.7
0.093456	92053.7	0.093402	84420.0
0.097921	71761.5	0.097973	52635.6

t(s)	P(0.1 Pa)	t(s)	P(0.1 Pa)
0.102233	95459.1	0.102306	227027.2
0.106745	29162466.0	0.106762	22536742.0
0.111206	37847500.0	0.111199	25862006.0
0.115640	31081492.0	0.115654	23281204.0
0.120101	17273878.0	0.120078	10737620.0
0.124513	3280914.0	0.124560	2446392.5
0.128983	1851316.2	0.128981	1427576.6
0.133436	1590965.0	0.133443	874073.9
0.137899	1565110.5	0.137881	967018.2
0.142350	1277844.8	0.142353	65290.2
0.146824	1448764.4	0.146834	1069732.5
0.151225	2404157.5	0.151232	1441442.9
0.155676	5860232.0	0.155687	4499368.0
0.160130	24175720.0	0.160127	16600458.0
0.164578	40694164.0	0.164584	24722026.0
0.169013	42539200.0	0.169019	25291488.0
0.173460	17903116.0	0.173474	14658130.0
0.177925	6884173.0	0.177940	1730901.6
0.182393	2095387.6	0.182388	1310679.0
0.186848	1858593.6	0.186817	841806.8
0.191240	1656174.4	0.191256	1149729.1
0.195735	2919797.5	0.195719	991107.4
0.200162	1262091.5	0.200127	696235.8

t(s)	P(0.1 Pa)	t(s)	P(0.1 Pa)
0.204578	2498959.5	0.204561	1265955.1
0.209082	3249241.0	0.209028	1976617.5
0.213513	17495244.0	0.213513	3897330.2
0.217955	31281572.0	0.217939	20548910.0
0.222395	44794604.0	0.222408	25360638.0
0.226848	29231886.0	0.226847	23645382.0
0.231301	18164938.0	0.231303	11133044.0
0.235732	2844548.8	0.235746	1921927.6
0.240195	1938333.0	0.240181	1239679.4
0.244665	1764875.2	0.244624	1191149.5
0.249066	1465020.5	0.249096	1053012.6
0.253532	1452452.1	0.253561	641967.8
0.257976	1489164.8	0.258000	982666.2
0.262437	2301855.8	0.262411	1397352.6
0.266882	7152683.0	0.266888	4621533.0
0.271342	24279252.0	0.271329	16744376.0
0.275773	38816980.0	0.275781	24627972.0
0.280220	39598012.0	0.280219	25101488.0
0.284663	23099832.0	0.284693	14615227.0
0.289141	5701273.0	0.289131	5632372.5
0.293589	2041681.6	0.293572	1486957.2
0.298027	1621922.9	0.298034	148010.9
0.302453	1471819.2	0.302488	1067791.1